nature materials

ARTICLES

https://doi.org/10.1038/s41563-021-01123-y

Check for updates

Engineering living and regenerative fungal–bacterial biocomposite structures

Ross M. McBee[1,2], Matt Lucht[3], Nikita Mukhitov[4], Miles Richardson[2,5], Tarun Srinivasan[1], Dechuan Meng[4], Haorong Chen[4], Andrew Kaufman[2], Max Reitman[3], Christian Munck[2], Damen Schaak[3]✉, Christopher Voigt[4] and Harris H. Wang[2,6]✉

Engineered living materials could have the capacity to self-repair and self-replicate, sense local and distant disturbances in their environment, and respond with functionalities for reporting, actuation or remediation. However, few engineered living materials are capable of both responsivity and use in macroscopic structures. Here we describe the development, characterization and engineering of a fungal–bacterial biocomposite grown on lignocellulosic feedstocks that can form mouldable, foldable and regenerative living structures. We have developed strategies to make human-scale biocomposite structures using mould-based and origami-inspired growth and assembly paradigms. Microbiome profiling of the biocomposite over multiple generations enabled the identification of a dominant bacterial component, *Pantoea agglomerans*, which was further isolated and developed into a new chassis. We introduced engineered *P. agglomerans* into native feedstocks to yield living blocks with new biosynthetic and sensing–reporting capabilities. Bioprospecting the native microbiota to develop engineerable chassis constitutes an important strategy to facilitate the development of living biomaterials with new properties and functionalities.

Fungal-based biomaterials have gained attention as unique scalable biocomposite materials with favourable mechanical and biodegradable properties[1,2]. To make fungal biocomposites, fungal mycelium is grown on a particulate or granular lignocellulosic feedstock material, such as stover or another agricultural waste product. Over the course of several days, the fungus partially consumes the feedstock material and infiltrates it, growing a dense hyphal mycelium network that binds together feedstock particles and fibres, thus forming the bulk biocomposite material[3]. Construction using fungal biocomposite objects, typically in the form of 'bricks', is sometimes referred to as 'mycotecture'. Fungal-based biomaterials have expanded into commercial markets and inspired new developments in sustainable biodesigns and fashion[4,5]. However, current fungal biocomposite products typically undergo a final inactivation process to heat-kill the living cells, thus rendering the material inert[3]. If instead the material is kept alive, there would be a greater opportunity to leverage the living components for manipulation, engineering and functionalization.

The emerging area of engineered living materials (ELMs) seeks to develop programmable living and responsive next-generation materials[6,7]. ELMs generally rely on embedding living cells in an organic or inorganic matrix, which provides the resulting bulk material with additional mechanical or functional properties. For instance, living cells can be embedded in synthetic organic polymers, resulting in biofunctionalized fibres[8], hydrogels[9] and nanomaterials[10]. The matrix can also be endogenously produced by the living component of the material itself, as in the case of engineered biofilms[11,12] or functionalized bacterial cellulose[13,14]. These materials can be programmed to exhibit complex behaviours such as antibiotic production[15], electrical conductivity[16], stimuli responsiveness[17,18] and mechanical actuation[19]. However, such ELMs often require complex bioreactors and post-processing steps to manufacture at scale[20,21]. On the other hand, biomineralization approaches have yielded biocomposites in which calcium-precipitating bacteria facilitate binding and stabilization of granular materials such as sand in a bioconcrete[22,23]. ELMs made with inorganic matrices can be produced at commercial scales[24], but are generally inert because the living components are entombed by their own precipitates and are not activated unless exposed to the environment[25].

Using a fungal biomaterial paradigm, we describe here the development of a living and self-healing biocomposite capable of forming human-scale architectural objects that can be functionalized with an engineered microbial component (Fig. 1a). We show the generation of brick-sized building blocks and demonstrate design strategies that leverage unique biomaterial behaviours to make origami-inspired[26] foldable forms for assembly into macroscopic structures. Detailed metagenomic analysis of different feedstocks revealed a robust bacterial component, the *Pantoea agglomerans* taxa, which was further isolated, characterized and developed into an engineerable chassis. Reintroducing a modified *P. agglomerans* back into the biocomposite enabled production of new molecules and synthetic sensing–signalling capabilities in situ. We envisioned that our *P. agglomerans* strain could serve as a versatile bacterial component of fungal–bacterial biocomposites that can be manipulated in the laboratory and redeployed in situ to expand the functionality of ELMs. More generally, engineering the microbiota that are natively associated with a material constitutes a compelling approach to develop new ELMs.

Construction of human-scale living biocomposite structures

Fungal biocomposites typically consist of lignocellulosic feedstock substrates bound together by fungal mycelium into a bulk

[1]Department of Biological Sciences, Columbia University, New York, NY, USA. [2]Department of Systems Biology, Columbia University, New York, NY, USA. [3]Ecovative Design, Green Island, NY, USA. [4]Department of Biological Engineering, Massachusetts Institute of Technology, Cambridge, MA, USA. [5]Integrated Program in Cellular, Molecular, and Biomedical Studies, Columbia University, New York, NY, USA. [6]Department of Pathology and Cell Biology, Columbia University, New York, NY, USA. ✉e-mail: damen@ecovativedesign.com; hw2429@columbia.edu

material. We chose to use a cosmopolitan white-rot fungi bracket fungus *Ganoderma* sp. as the fungal mycelium for our biomaterial. *Ganoderma* can subsist on a wide variety of lignocellulosic biomass using diverse lignin-degrading enzymes[27], thus making them an ideal species for use in biocomposites. We first explored fibrous particulates derived from hemp hurd as an organic substrate to build *Ganoderma* sp. biocomposites. We mixed this substrate with *Ganoderma* sp. mycelial starter culture inoculum, typically at a ratio of 1:1 inoculum to feedstock by wet weight, along with water and small amounts of flour and calcium sulfate as nutritional supplement (see Methods). Due to the metabolic flexibility of *Ganoderma* sp., the substrate could be used 'raw' and did not need to be pre-sterilized to allow for robust fungal growth. The resulting moist aggregate was readily shaped in moulds, where the fungus grew into the feedstock material, binding it together. After 5–7 days of fungal growth and mycelial infiltration of the substrate (Extended Data Fig. 1), the form-stable object was removed from the mould for further assembly into larger structures as needed. The final structure was desiccated in ambient conditions to a final density of ~120 kg m^{-3}. A simple illustration of this fungal biocomposite growth paradigm is the generation of a brick in a preformed plastic mould (Fig. 1b). The resulting bricks can have dimensions of up to around 20 × 20 × 40 cm, on a par with standard concrete masonry units (for example, a cinderblock), provided that proper aeration and hydration is maintained during the material growth phase, and have predictable bulk material properties (Extended Data Fig. 2 and Supplementary Table 1).

The ability of *Ganoderma* sp. to grow on raw feedstocks suggests possibilities for new and versatile growth paradigms. Because the throughput of biomaterial manufacturing using individual moulds is limited by the availability of moulds at any given time, we have designed a flat-pack paradigm that relies on the assembly of slotted pre-cut sheets to form grids of moulds into which the fungal–substrate mixture can be placed for growth (Fig. 1b). The sheets are made from cheap, lightweight and biodegradable wax-coated cardboard that can be readily manufactured at an industrial scale or on demand (for example, with a blade), easily stacked for transportation and simply assembled to make moulds for brick-like blocks with mechanical characteristics comparable to those grown in plastic moulds. Beyond simple rectangular prism bricks, more complex geometries can also be easily manufactured by introducing curves into mould partitions (Fig. 1c). This flat-pack mould design allows for the generation of complex block subunits and planar forms from flat-pack moulds.

Because fungal mycelia dominate the living biomass of the biocomposite and remain metabolically active throughout the growth and desiccation phases, they provide unique capabilities for fusion and repair. Living blocks placed in physical contact with one another will fuse together, thus allowing for the mortarless assembly of biomaterial objects into more complex structures. Using this approach, we constructed a human-scale arch from dumbbell-shaped subunit blocks grown over the course of 33 days (5-day growth, 7-day fusion and 3-week desiccation; Fig. 1c). This structure is self-supporting once fused, and composed entirely of fused blocks without any additional internal reinforcement. Similarly, broken or damaged blocks can be healed or reformed by placing fractured pieces in contact and allowing regrowth and fusion, or by the addition of filler myceliated substrate to bridge larger gaps and seal larger wounds. Healed materials can resist subsequent fracture at the repaired site and retain most, if not all, of the original mechanical properties (Fig. 1c).

The final moulded block is a contiguous solid with low mechanical flexibility that requires piecemeal assembly to form larger structures. We thus sought to explore ways to build foldable blocks that would allow for kinematic assembly to generate sophisticated geometries with a pre-specified design and minimal in-field assembly, beginning with a simple hinge. Because *Ganoderma* sp. can grow on diverse substrates, including structured organic matter such as fabrics and matting, we tested the use of such flexible material to physically connect blocks (Fig. 1d). A 'living hinge' was made by placing hemp mat material at a junction between two moulding blocks during the material growth phase. The matting became integrated into the living element as the fungus grew, thus providing embedded flex and hinge points in the resulting object. Using this principle, we designed more sophisticated structures, including a box and an arch, which could be flat-pack moulded and grown on a two-dimensional (2D) surface and then erected into its designated three-dimensional form (Fig. 1d and Extended Data Fig. 3). The final structures become stable upon material self-fusion at the hinge seams. This kinematic construction and assembly approach accommodates the generation of pop-up and origami-like structures with much greater sophistication than is possible using simple elemental building blocks, while allowing for complex forms to be pre-specified in the design of the slot-together moulds.

Biocomposite objects or structures can be ground back into particulate material to serve as fungal inoculum with additional, new unsterilized feedstock for further iterative expansion of the biomaterial. Each full generation cycle of the material can take up to 30 days, or as short as 5 days, depending on whether freshly demoulded or fully desiccated material is used as the new inoculum (Fig. 2a). With this regeneration strategy, we have passaged the biocomposite for four full generations without any measurable loss of material strength (Extended Data Fig. 3). We have been able to reprocess biocomposite objects up to a month after block desiccation without issue. After a year in open ambient conditions, the *Ganoderma* sp. can still be resurrected from the material in rich media. However, new blocks seeded with very old blocks as inoculum are more prone to the growth of contaminant species (Extended Data Fig. 3). Together, these results demonstrate the generation of a multifunctional fungal-based biocomposite that can be robustly grown using raw feedstocks and moulded into various building blocks or kinematic assemblies.

Characterization of fungal biomaterial biodiversity

Because the living biomaterial uses raw non-sterile feedstocks, the diverse microbial and fungal components present in the biocomposite or its feedstocks may exhibit complex spatiotemporal

Fig. 1 | Development of a versatile fungal–bacterial living material. a, A schematic outlining the design and functionalization of the fungal–bacterial biocomposites in this study. **b**, The fungal mycelium of *Ganoderma* sp. is mixed with raw feedstock and placed in plastic precast vacuform moulds or in flat-pack slot-together moulds made from wax-coated cardboard to produce lightweight yet strong biocomposite blocks that can be assembled into larger structures. The strength bar graph shows the mean, with error bars showing the standard deviation (SD) of a standard compressive strength test to failure. The objects produced with cardboard moulds have similar strengths to those generated using conventional plastic moulds. **c**, Building blocks with curved geometries can be generated and used to build arches by self-fusion. Broken blocks will self-repair over time when fragments are placed in physical contact. Healed material (grown in a controlled humidity of >60%) has similar physical characteristics to the original material. Similarly, backfilling of a punctured hole with fresh biomaterial enables robust wound repair with strong mechanical resistance to further fractures. The bar graphs show the mean with SD error bars for a standard three-point bend test measuring tensile strength. **d**, Flexible connectors made from cloth or matting enable the joining of biocomposite block units, yielding 'living hinges' that can be used to build more sophisticated structures by kinematic and origami-inspired assembly paradigms. Upon assembly, the hinges naturally fuse together to form the final stable structure. Scale bar, 30.48 cm; the box is 30.48 × 30.48 × 30.48 cm.

growth dynamics that could affect the physical or functional performance of the resulting material. We therefore profiled the microbiome of the raw feedstocks and biomaterials generated using three agricultural byproducts, namely corn stover, shredded canola and hemp hurd, for different inoculation ratios (that is, the wet-weight ratio of feedstock to the *Ganoderma* sp. inoculum). We first performed 16S amplicon sequencing and found that the bacterial microbiomes were more similar between samples from

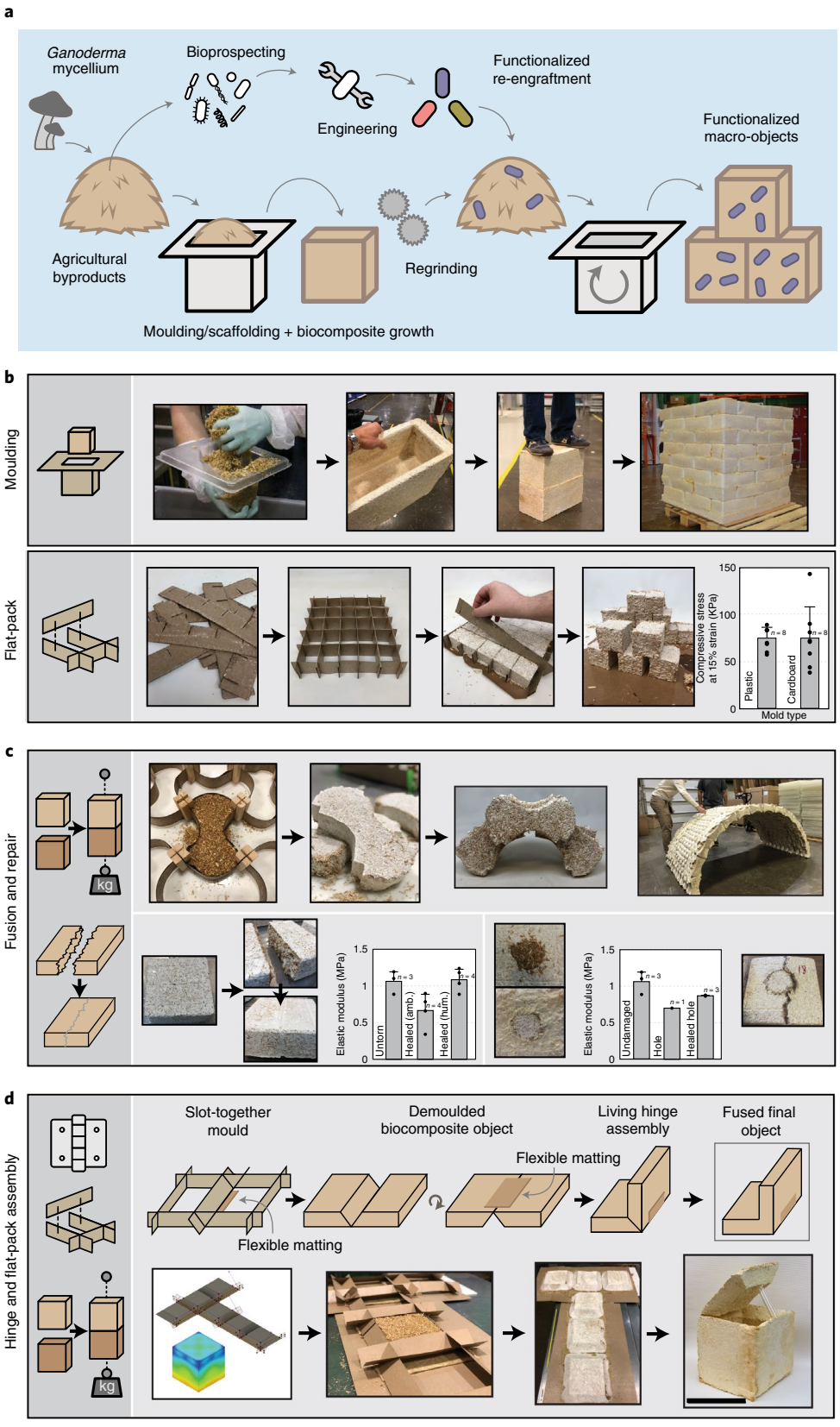

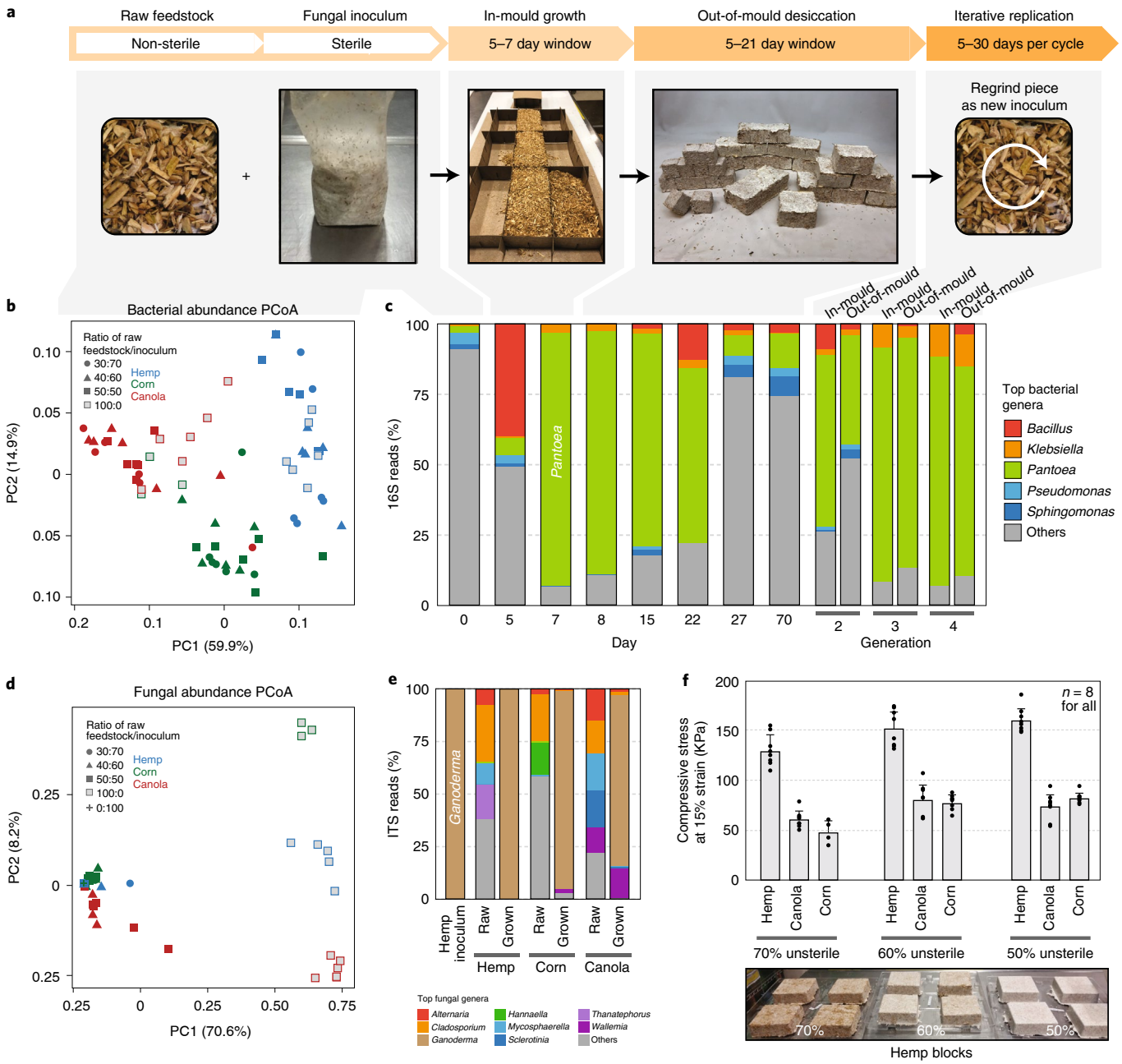

Fig. 2 | Biocomposite generation and metagenomic characterization. a, An outline of a generation cycle of the biocomposite. Sterile *Ganoderma* sp. inoculum is combined with raw non-sterile feedstock and placed in a mould for in-mould growth for 5–7 days. The form-stable moulded biocomposite is removed from the mould and allowed to desiccate out-of-mould for 5–21 days. Desiccated and non-desiccated material can be reground and used to seed raw feedstocks for the generation of additional biocomposites. **b**, Principal coordinate analysis (PCoA) of the bacterial microbiome from biomaterials generated using different feedstocks and inoculation ratios (30:70, 40:60 and 50:50) compared with raw feedstock (100:0) using 16S amplicon sequencing. **c**, Taxonomic assignment of 16S reads from a biomaterial sampled during different phases of growth, showing a dominant *Pantoea* taxa. **d**, PCoA of the fungal microbiome from the same biomaterials as in **b** using metagenomic ITS sequencing, as well as pure inoculum. **e**, Taxonomic assignment of ITS reads from biomaterial grown with different feedstocks, showing a dominant *Ganoderma* population. **f**, Compressive strengths of blocks grown from different feedstocks with varying ratios of feedstock to fungal inoculum. The bar graph shows the mean, and the error bars show the SD.

each substrate regardless of inoculation ratio than between different substrates (Fig. 2b). Distinct communities of *Pantoea* and *Pseudomonas* dominated the hemp biomaterials, whereas *Saccharopolyspora* and *Staphylococcus* dominated the canola and *Sphingomonas* dominated the corn biomaterials (Extended Data Fig. 4). We then temporally profiled the bacterial community of a hemp-grown biomaterial during an entire generation cycle, starting with the initial inoculum to the final desiccated block, and over several subsequent generations (Fig. 2c). One γ-proteobacteria taxa, belonging to the *Pantoea* genus, exhibited robust and reproducible blooms during the biomaterial growth and desiccation phases, remained dominant throughout multiple generations and was enriched across different spatial locations throughout the biomaterial blocks (Extended Data Fig. 4).

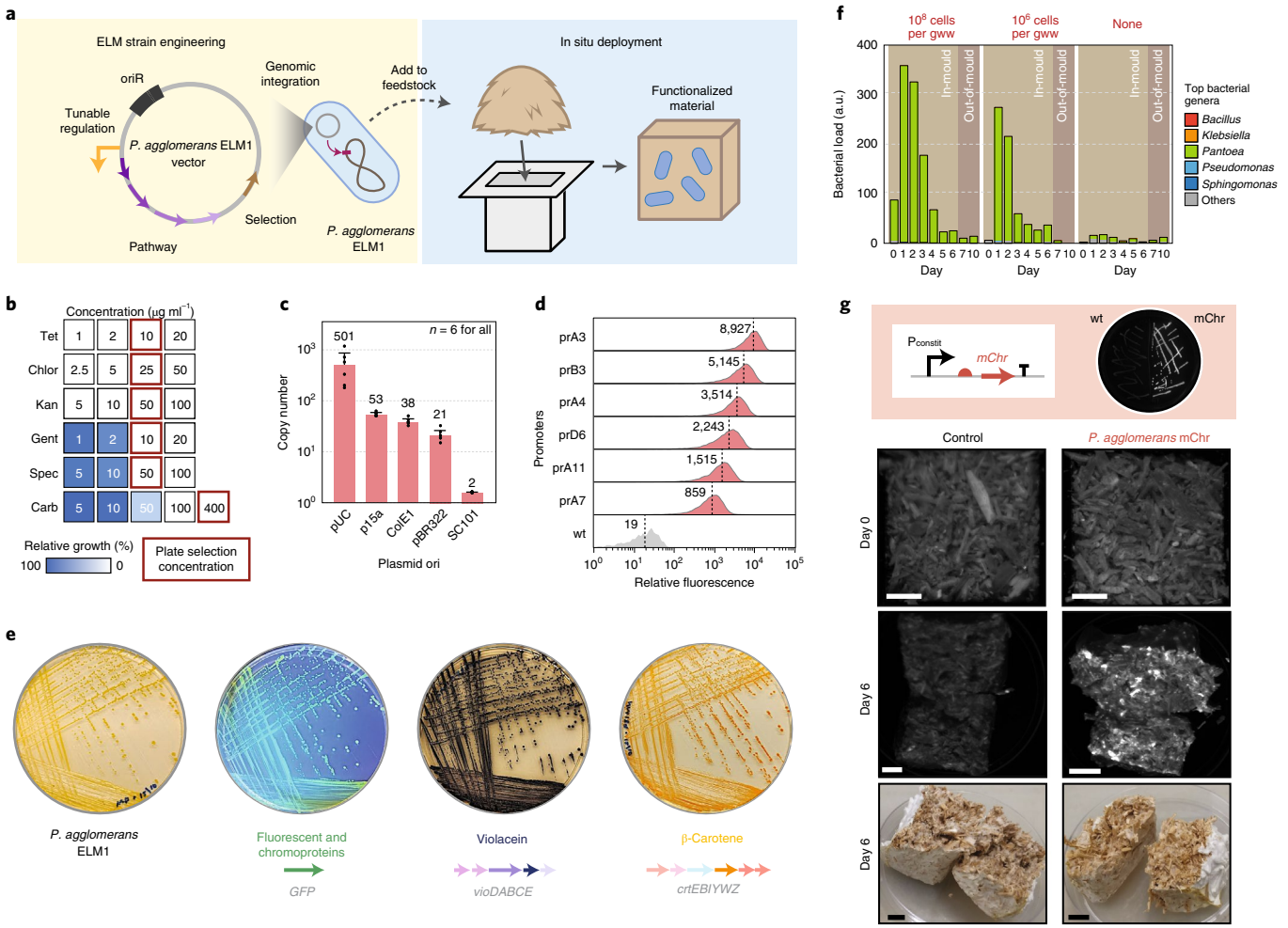

Fig. 3 | Bioprospecting and engineering of a native bacterial component of the biocomposite. a, Schematic showing the development of a genetic engineering and synthetic biology toolbox for *P. agglomerans* ELM1 (left) and the redeployment of engineered *P. agglomerans* back into a biomaterial (right). **b**, Antibiotic sensitivity of *P. agglomerans* ELM1 and concentrations that were used to select recombinant *P. agglomerans* ELM1 containing the corresponding resistance gene. **c**, Plasmid copy numbers across various origins of replication in *P. agglomerans* ELM1. The bar graph shows the mean, and the error bars represent the SD. **d**, Characterization of constitutive promoters using a GFP reporter in *P. agglomerans* ELM1. Each row represents the flow cytometry of a colony carrying a GFP expression plasmid driven by the promoter in question, compared with wild-type, untransformed *P. agglomerans* ELM1 cells (wt). **e**, Successful introduction of reporter genes and biosynthetic pathways into *P. agglomerans* ELM1. **f**, Viability of exogenously introduced *P. agglomerans* into a living block showing the dosage-dependent expansion of *P. agglomerans* during the in-mould growth phase. The bacterial load is proportional to the absolute abundance of a given taxon (see Methods). The dosing is *P. agglomerans* colony-forming units per gww. living material prior to growth. **g**, Re-engraftment of modified *P. agglomerans* ELM1 containing an mCherry reporter driven by a constitutive BBaJ23100 promoter (referred to as 'Pconstit' in the figure) into a living biocomposite showing an mCherry signal after 6 days of biomaterial growth. The 5.08 × 5.08 × 5.08 cm blocks were shown broken open and imaged using a ChemiDoc imager to visualize fluorescence engraftment. The experiment was repeated independently to confirm this result. Scale bars, 1.27 cm.

Because the majority of the living biomass is composed of the fungal component, we also performed metagenomic internal transcribed spacer (ITS) sequencing to assess the fungal microbiome of the biomaterials grown with different substrates. Similar to the bacterial communities, each feedstock had distinct mycobiomes prior to inoculation (Fig. 2d). However, once inoculated and grown with *Ganoderma* sp., the biocomposites were dominated almost exclusively by *Ganoderma* sp., although canola also showed a certain level of *Wallemia* groups (Fig. 2e). These mycobiome differences suggest that *Ganoderma* sp. robustly outcompetes the native fungal species in the feedstock, which may be facilitated by *Pantoea* growth. Further compressive strength testing of the blocks generated at different inoculation ratios for the three feedstocks revealed that the hemp-based biomaterials were stronger than those made with corn and canola (Fig. 2f). *Ganoderma* sp. seeding levels affected the speed of material development and its mechanical properties, with a 50% or 1:1 feedstock-to-inoculum ratio providing the best and most robust material generation after 5 days of in-mould growth. Together, these results indicate that for the best-performing biocomposite made from hemp substrates, the microbial community within the biomaterial is predictable and spatially stable, dominated by the *Ganoderma* sp. fungal component and a *Pantoea* spp. bacterial component.

Bioprospecting a bacterial chassis from the living material

Pantoea spp. are soil-associated microbes found prevalently in the rhizosphere, as well as in insects and in the intestinal tract of various plant-feeding livestock[28]. Given the robust growth and dominance of *Pantoea* in our fungal hemp-based biocomposite, we therefore explored the possibility of developing an engineerable

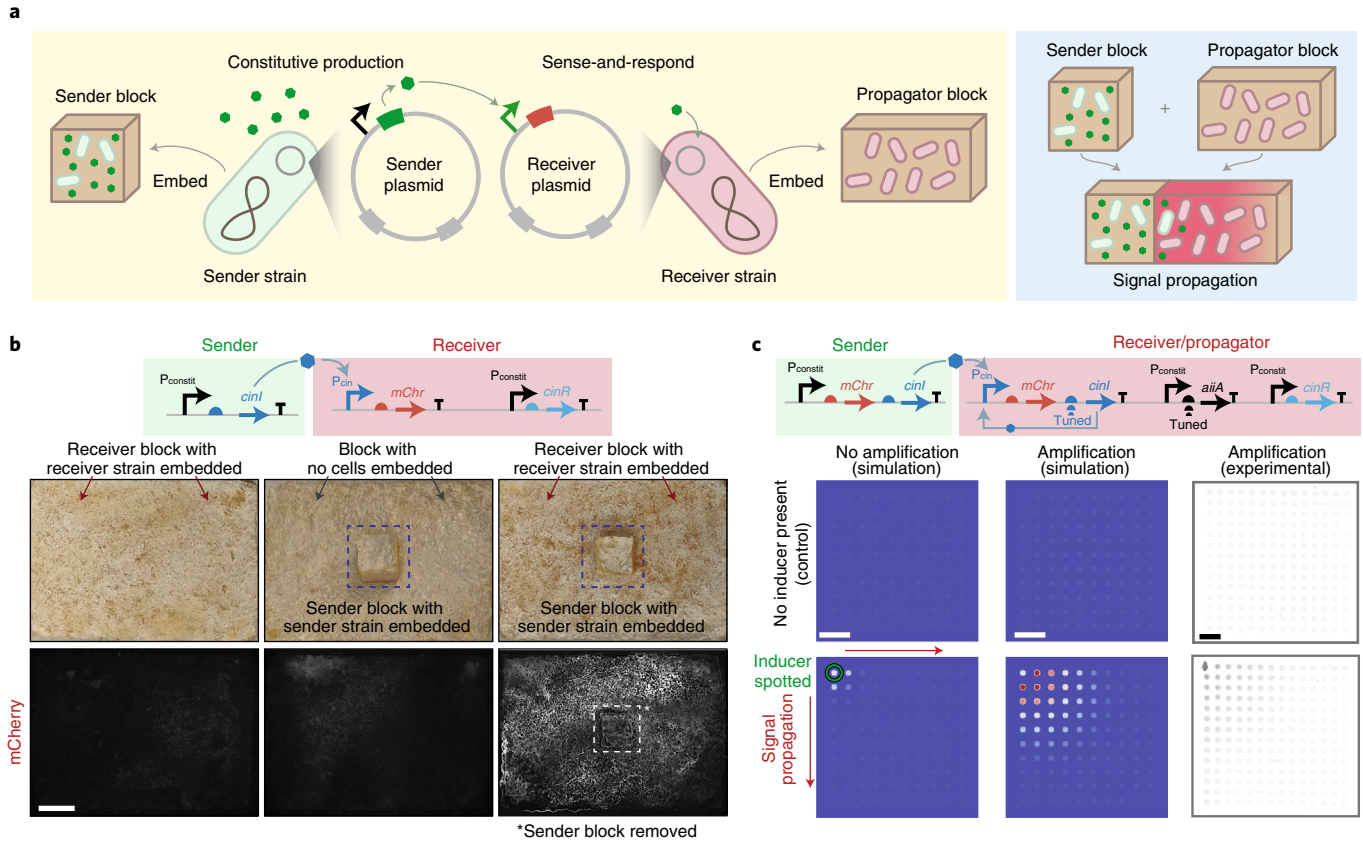

Fig. 4 | Developing a stimuli-responsive living material. a, A schematic of the functionalization of a stimuli-responsive ELM with engineered *P. agglomerans* ELM1, showing the *P. agglomerans* ELM1 sender and propagator strains (left) and the responsive bulk material (right) **b**, A *P. agglomerans* ELM1 'sender' strain is embedded in a sender block and produces a signalling molecule, AHL. When the sender block is placed in contact with a block containing a 'receiver' strain and rehydrated, the receiver block produces mCherry in response to the AHL signal. This experiment was successfully repeated to confirm this result. Note that the sender block is removed from the receiver block before imaging, although prior contact leaves a small shadow. P_{cin}, AHL responsive promoter. Scale bar, 5 cm (for all images). **c**, A feed-forward sense-and-respond communication circuit can further enhance signal propagation in the block. In silico simulation of signal propagation potential after inducer activation is shown in the left two sets of blue panels, and experimental testing of communication circuits in *P. agglomerans* ELM1 along a 2D agar surface is presented in the right set of panels, showing increased and sustained signal propagation. Panels above **b** and **c** are schematic representations of the genetic circuits being tested, showing differences in architecture between initial and feed-forward designs. Scale bars, 5 mm (for all images).

Pantoea chassis that could be used to install new functionality into our biocomposite for ELM applications (Fig. 3a). This approach contrasts with past attempts to place laboratory-adapted bacteria in natural settings where they often fail to persist, which is a common challenge in many probiotic engineering applications[29]. We isolated 33 candidate bacterial strains from the hemp feedstock, belonging mostly to *Bacillus* and *Pantoea* genera (Extended Data Fig. 5), and selected one *Pantoea* isolate for further study, which we designated *P. agglomerans* ELM1. We performed essential phenotypic characterizations on *P. agglomerans* ELM1 and built a suite of genetic tools to support its genetic manipulation. *P. agglomerans* ELM1 could grow robustly in rich media such as lysogeny broth (LB) and yeast-tryptone (YT) (a doubling time of ~50 min at 30 °C), as well as in media prepared by boiling the hemp feedstock in water (Extended Data Fig. 6). M9 minimal media supplemented with different carbon sources could also support some level of *P. agglomerans* ELM1 growth (Extended Data Fig. 6). The strain exhibited natural resistance to gentamycin (Gent), spectinomycin (Spec) and carbenicillin (Carb), but susceptibility to other antibiotics, including tetracycline (Tet), chloramphenicol (Chlor) and kanamycin (Kan; Fig. 3b). Nonetheless, most standard antibiotic concentrations commonly used in the laboratory were sufficient for robust selection in both solid and liquid media, which could be rescued using different antibiotic resistance genes (Extended Data Fig. 6).

Whole genome sequencing of *P. agglomerans* ELM1 yielded a 4.08 Mb complete and closed genome as well as two very large plasmids (535 and 208 kb; Extended Data Fig. 7). The *P. agglomerans* ELM1 genome is most closely related to a *P. agglomerans* L15 genome (RefSeq: NZ_CP034148.1), with an average nucleotide identity (ANI) of 98.89% at the genome level. Analysis of the *P. agglomerans* ELM1 genome revealed a variety of genomic signatures that could be contributing to the strain's ability to thrive on the lignocellulosic hemp feedstock and compete in the living biocomposite, including spectinomycin and carbenicillin resistance genes (Supplementary Tables 2–4), a large suite of carbohydrate-active enzymes (CAZymes), including cellulases and lignin degrading genes (Supplementary Table 5), as well as several quorum-sensing-related clusters and a putative phenazine antibiotic production and resistance cluster, carried on one of the plasmids (Extended Data Fig. 7).

To develop a more comprehensive genetic toolkit for *P. agglomerans* ELM1, we tested the transformation protocols of different plasmids by electroporation and selection for transformants (Extended Data Fig. 8, also see Methods). Transformants with plasmids containing different origins of replication had similar plasmid copy

numbers as in other model bacteria such as *Escherichia coli* (Fig. 3c). An *E. coli* carrying an RK2 conjugative plasmid could also be used to deliver plasmids to *P. agglomerans* ELM1 by conjugation (Extended Data Fig. 8). Foreign DNA could also be stably integrated into the *P. agglomerans* ELM1 genome at its native attTn*7* site using a Tn*7*-based transposition system[30] (Extended Data Fig. 8). We further expressed a GFP reporter from different regulatory elements in the strain to yield promoters with varying levels of expression strengths (Fig. 3d and Extended Data Fig. 9). Finally, we introduced more complex multigene pathways into *P. agglomerans* ELM1 to produce non-native metabolites, including canthaxanthin and violacein[31] (Fig. 3e and Extended Data Fig. 9), which has antimicrobial properties that could help provide resistance to microbial contamination.

We next tested whether inoculating an engineered *P. agglomerans* ELM1 back into the feedstock resulted in re-engraftment of the bacterium into the bulk material, and whether reintroduced recombinant strains could produce proteins in situ. *P. agglomerans* ELM1 was spiked back into the hemp feedstock at different seeding levels along with the *Ganoderma* sp. inoculum, and the growing biomaterials were assessed by absolute abundance 16S amplicon sequencing[32]. We found that reintroducing *P. agglomerans* ELM1 at concentrations comparable to those found in soil communities could dramatically boost *Pantoea* levels in the material (Fig. 3f and Extended Data Fig. 10), even without nutritional supplementation or antibiotic selection. Using a modified *P. agglomerans* ELM1 strain carrying an mCherry-expressing plasmid in media with antibiotic supplementation, we were able to generate a biocomposite block that exhibited mCherry fluorescence throughout the biomaterial after 6 days of growth (Fig. 3g) at a loading rate of about 10^9 *Pantoea* cells per gram wet weight (gww) of biocomposite. Similarly, a spike-in of *P. agglomerans* ELM1 carrying a violacein-producing plasmid yielded visibly purple blocks with no noticeable effect on fungal growth (Extended Data Fig. 10). This new suite of genetic tools and the demonstrated re-engraftment back into raw feedstocks greatly expand the relevance of *P. agglomerans* ELM1 as an ELM chassis for our fungal–bacterial biocomposite.

Towards a living responsive fungal–bacterial biocomposite

In contrast to inert objects, living systems can sense stimuli locally and transmit that signal through signal transduction networks to other distal parts of their bodies to produce a response. We therefore sought to mimic such capabilities in our ELM to build sensing and responsive living materials (Fig. 4a).

To explore whether signal detection within the bulk material was possible, we built a stimuli-responsive *P. agglomerans* strain that expresses an mCherry fluorescent reporter in response to a quorum molecule (acyl homoserine lactone, AHL). Blocks containing this 'receiver' strain were fluorescent when grown with AHL included in the block recipe (Extended Data Fig. 10). We then constructed a separate 'sender' *P. agglomerans* strain capable of constitutively producing AHL. Together, these strains constitute a simple prototypical intercellular signalling system (Fig. 4b). We introduced the sender and receiver strains into separate feedstocks and generated sender and receiver biocomposite blocks. When the sender block is placed in contact with the receiver block and rehydrated with media, the AHL signal molecules generated from the sender block can diffuse into the receiver block and induce mCherry expression. Indeed, we only observed mCherry expression in the receiver block after co-incubation of the sender and receiver blocks for 16 h (Fig. 4b).

Given that the signal molecule from sender cells can only travel a limited distance by diffusion before signal degradation and loss, we explored a receiver design that can robustly amplify and further propagate the signal upon initial induction (that is, a 'receiver propagator'). To accomplish this signalling design, we introduced a feed-forward loop into the receiver circuit to produce additional AHL upon initial activation of the receiver circuit (Fig. 4c). Newly generated AHL molecules can reach neighbouring receiving cells, thereby 'rebroadcasting' the signal to further propagate the signal across the receiver population. To avoid runaway accumulation of AHL molecules, the receiver-propagator cells were also designed to constitutively express an *aiiA* gene that encodes an enzyme responsible for the hydrolysis of AHL molecules[33], thereby inactivating it. The sensitivity and performance of this system depend on the expression and activity of the AHL synthase cinI and aiiA. Through in silico simulations of the receiver-propagator circuit parameters, we verified that the feed-forward loop design is feasible and could avoid runaway autoactivation by AHL (see Methods). We then constructed different receiver-propagator circuits with a library of *aiiA* and *cinI* ribosomal binding sites (RBSs) of different strengths to test for the optimal performing circuit. The receiver-propagator system could transmit and amplify an initial signal across large distances while avoiding erroneous self-activation (Fig. 4c). When *P. agglomerans* ELM1 cells carrying the receiver-propagator plasmid were spiked into a biomaterial block and induced by the addition of AHL solution to the surface of the biomaterial before growth, the resulting blocks showed mCherry fluorescence after 6 days of growth, although the strength of fluorescence was low compared with constitutive mCherry expression (Extended Data Fig. 10). The weaker fluorescence signal may be due to *P. agglomerans* existing in a stationary growth phase in the block, or the lack of sufficient cell density required for repropagating the signal to neighbouring cells to robustly activate the receiver-propagator circuit. Nevertheless, these results highlight a signalling system that can generate a signal from sender cells that induces the expression of a reporter molecule in receiver cells as well as further amplifying the signalling molecule, pointing the way towards sustained signal amplification and transduction throughout a receiver block after a locally sensed stimulus.

Outlook

Fungal-based biocomposites represent a versatile class of high-performance, lightweight and biodegradable materials. Compared with strategies for forming fungal biocomposites that rely on the use of sterilized feedstocks, our approach relies on the key natural functionalities of the living material, including its ability to grow on raw feedstocks, its easy moulding into diverse solid or foldable shapes and structures, and its self-fusion and self-repair properties. The demonstration of robust material generation using non-sterile feedstocks greatly expands the relevance of this biocomposite for mass in-field production in resource-limited settings. The ability to regrind old material and use it as 'diluted' inoculum with new feedstock also allows for the generation of more working material. At an inoculation ratio of one-part reground biocomposite to one-part new feedstock, the initial amount of inoculum can be expanded over 30-fold in 30 days. Using a first-generation block as dried inoculum and scavenged feedstock, this would allow for the generation of 100 living material 'cinderblocks' of the type shown in Fig. 1b with just a single 35-cm-a-side, 5-kg block of starting inoculum. Similarly, the isolated engineered *Pantoea* strain can be grown on diverse media, including those derived from hemp feedstock or traditional laboratory media. We envision that future versions of this material would be well-suited to medium-term use in resource-limited settings such as disaster relief, where it could be used to construct living structures from materials gathered on-site using easily manufactured and transported prepatterned slot-together folding forms to minimize labour. These living structures might sense and respond to a variety of environmental signals relevant in such settings, such as heavy metals or cholera toxin present in the water supplies used to build the structure. And, once they are no longer needed, these structures can naturally biodegrade with minimal long-term impact on the local environment.

Several outstanding challenges require further attention. For one, the need for material hydration for adaptive biological response is an important limitation because desiccated material states support less actively growing, sensing and responsive cells. Further engineering of *P. agglomerans* for the in situ production of violacein or native phenazines could be promising strategies for reducing unwanted bioburden and contamination. Better reporter systems for direct readout from the biomaterial could also improve input/output signal transmission of the material because the fungal mycelium allows optical-based measurements (for example, fluorescence) only in a shallow surface layer of the material. Strategies such as the use of diffusible and volatile compounds as reporters or cellular recording systems[34] could provide alternative modality for tracking the biomaterial state. For use in out-of-the-lab scenarios, the biocontainment of genetically engineered material components is important[35]. In such cases, engineered auxotrophy of the *P. agglomerans* strain and supplementation of the material, or a fungal metabolite-responsive growth regulating sensor would be useful further developments.

The approach described here represents a prototypical strategy to generate an ELM. We envision that future fungal biomaterials will possess new functionalities, such as the capacity to produce protective molecules to reduce ultraviolet damage[36], make on-demand compounds, including foods and pharmaceuticals, and sense and react to pollutants, toxins or other biological or chemical threats from the environment[17]. These biomaterials could be used for diverse areas of application, such as wearable products, distributed environmental sensors or smart living quarters suitable for human habitation.

Online content

Any methods, additional references, Nature Research reporting summaries, source data, extended data, supplementary information, acknowledgements, peer review information; details of author contributions and competing interests; and statements of data and code availability are available at https://doi.org/10.1038/s41563-021-01123-y.

Received: 7 November 2020; Accepted: 7 September 2021;
Published online: 02 December 2021

References

1. Haneef, M. et al. Advanced materials from fungal mycelium: fabrication and tuning of physical properties. *Sci. Rep.* **7**, 41292 (2017).
2. Jones, M., Mautner, A., Luenco, S., Bismarck, A. & John, S. Engineered mycelium composite construction materials from fungal biorefineries: a critical review. *Mater. Des.* **187**, 108397 (2020).
3. Elsacker, E. et al. A comprehensive framework for the production of mycelium-based lignocellulosic composites. *Sci. Total Environ.* **725**, 138431 (2020).
4. Silverman, J., Cao, H. T. & Cobb, K. Development of mushroom mycelium composites for footwear products. *Cloth. Text. Res. J.* **38**, 119–133 (2020).
5. Attias, N. et al. Mycelium bio-composites in industrial design and architecture: comparative review and experimental analysis. *J. Clean. Prod.* **246**, 119037 (2020).
6. Gilbert, C. & Ellis, T. Biological engineered living materials: growing functional materials with genetically programmable properties. *ACS Synth. Biol.* **8**, 1–15 (2019).
7. Nguyen, P. Q., Courchesne, N. M. D., Duraj-Thatte, A., Praveschotinunt, P. & Joshi, N. S. Engineered living materials: prospects and challenges for using biological systems to direct the assembly of smart materials. *Adv. Mater.* **30**, e1704847 (2018).
8. Townsend-Nicholson, A. & Jayasinghe, S. N. Cell electrospinning: a unique biotechnique for encapsulating living organisms for generating active biological microthreads/scaffolds. *Biomacromolecules* **7**, 3364–3369 (2006).
9. Gonzalez, L. M., Mukhitov, N. & Voigt, C. A. Resilient living materials built by printing bacterial spores. *Nat. Chem. Biol.* **16**, 126–133 (2020).
10. Charrier, M. et al. Engineering the S-layer of *Caulobacter crescentus* as a foundation for stable, high-density, 2D living materials. *ACS Synth. Biol.* **8**, 181–190 (2019).
11. Nguyen, P. Q., Botyanszki, Z., Tay, P. K. R. & Joshi, N. S. Programmable biofilm-based materials from engineered curli nanofibres. *Nat. Commun.* **5**, 4945 (2014).
12. Chen, A. Y. et al. Synthesis and patterning of tunable multiscale materials with engineered cells. *Nat. Mater.* **13**, 515–523 (2014).
13. Walker, K. T., Goosens, V. J., Das, A., Graham, A. E. & Ellis, T. Engineered cell-to-cell signalling within growing bacterial cellulose pellicles. *Microb. Biotechnol.* **12**, 611–619 (2019).
14. Caro-Astorga, J., Walker, K. T., Herrera, N., Lee, K.-Y. & Ellis, T. Bacterial cellulose spheroids as building blocks for 3D and patterned living materials and for regeneration. *Nat. Commun.* **12**, 5027 (2021).
15. Gerber, L. C., Koehler, F. M., Grass, R. N. & Stark, W. J. Incorporation of penicillin-producing fungi into living materials to provide chemically active and antibiotic-releasing surfaces. *Angew. Chem. Int. Ed.* **51**, 11293–11296 (2012).
16. Seker, U. O., Chen, A. Y., Citorik, R. J. & Lu, T. K. Synthetic biogenesis of bacterial amyloid nanomaterials with tunable inorganic–organic interfaces and electrical conductivity. *ACS Synth. Biol.* **6**, 266–275 (2017).
17. Tay, P. K. R., Nguyen, P. Q. & Joshi, N. S. A synthetic circuit for mercury bioremediation using self assembling functional amyloids. *ACS Synth. Biol.* **6**, 1841–1850 (2017).
18. Liu, X. et al. Stretchable living materials and devices with hydrogel–elastomer hybrids hosting programmed cells. *Proc. Natl Acad. Sci. USA* **114**, 2200–2205 (2017).
19. Chen, X., Mahadevan, L., Driks, A. & Sahin, O. *Bacillus* spores as building blocks for stimuli-responsive materials and nanogenerators. *Nat. Nanotechnol.* **9**, 137–141 (2014).
20. Cheng, H. P., Wang, P. M., Chen, J. W. & Wu, W. T. Cultivation of *Acetobacter xylinum* for bacterial cellulose production in a modified airlift reactor. *Biotechnol. Appl. Biochem.* **35**, 125–132 (2002).
21. Dorval Courchesne, N.-M., Duraj-Thatte, A., Tay, P. K. R., Nguyen, P. Q. & Joshi, N. S. Scalable production of genetically engineered nanofibrous macroscopic materials via filtration. *ACS Biomater. Sci. Eng.* **3**, 733–741 (2016).
22. Heveran, C. M. et al. Biomineralization and successive regeneration of engineered living building materials. *Matter* **2**, 481–494 (2020).
23. Castro-Alonso, M. J. et al. Microbially induced calcium carbonate precipitation (MICP) and its potential in bioconcrete: microbiological and molecular concepts. *Front. Mater.* **6**, 126 (2019).
24. BioMASON https://biomason.com (2020).
25. Botusharova, S., Gardner, D. & Harbottle, M. Augmenting microbially induced carbonate precipitation of soil with the capability to self-heal. *J. Geotech. Geoenviron. Eng.* **146**, 04020010 (2020).
26. Chen, Y., Peng, R. & You, Z. Origami of thick panels. *Science* **349**, 396–400 (2015).
27. Pinto, P. A. et al. Influence of ligninolytic enzymes on straw saccharification during fungal pretreatment. *Bioresour. Technol.* **111**, 261–267 (2012).
28. Walterson, A. M. & Stavrinides, J. *Pantoea*: insights into a highly versatile and diverse genus within the Enterobacteriaceae. *FEMS Microbiol. Rev.* **39**, 968–984 (2015).
29. Sheth, R. U., Cabral, V., Chen, S. P. & Wang, H. H. Manipulating bacterial communities by in situ microbiome engineering. *Trends Genet.* **32**, 189–200 (2016).
30. McKenzie, G. J. & Craig, N. L. Fast, easy and efficient: site-specific insertion of transgenes into Enterobacterial chromosomes using Tn7 without need for selection of the insertion event. *BMC Microbiol.* **6**, 39 (2006).
31. Furubayashi, M. et al. A highly selective biosynthetic pathway to non-natural C50 carotenoids assembled from moderately selective enzymes. *Nat. Commun.* **6**, 7534 (2015).
32. Ji, B. W. et al. Quantifying spatiotemporal variability and noise in absolute microbiota abundances using replicate sampling. *Nat. Methods* **16**, 731–736 (2019).
33. Dong, Y. H., Xu, J. L., Li, X. Z. & Zhang, L. H. AiiA, an enzyme that inactivates the acylhomoserine lactone quorum-sensing signal and attenuates the virulence of *Erwinia carotovora*. *Proc. Natl Acad. Sci. USA* **97**, 3526–3531 (2000).
34. Sheth, R. U., Yim, S. S., Wu, F. L. & Wang, H. H. Multiplex recording of cellular events over time on CRISPR biological tape. *Science* **358**, 1457–1461 (2017).
35. Lee, J. W., Chan, C. T. Y., Slomovic, S. & Collins, J. J. Next-generation biocontainment systems for engineered organisms. *Nat. Chem. Biol.* **14**, 530–537 (2018).
36. Martinez, L. M., Martinez, A. & Gosset, G. Production of melanins with recombinant microorganisms. *Front. Bioeng. Biotechnol.* **7**, 285 (2019).

Methods

Biomaterial feedstocks. Canola and corn were sourced from Aden Brook Agri Sales. Canola and corn were naturally harvested, then milled and binned for size: 1.9 cm canola straw and 3–38 mm corn stover. Naturally harvested decorticated hemp hurd, with a size range of 12–40 mm, was provided courtesy of Ecovative Design.

Growth and characterization of biomaterial. Hemp biocomposite objects were generated in a 'generational' fashion, whereby the initial object was grown from a mixture of 'primary' inoculum, grown on a sterilized feedstock to ensure robust colonization, and non-sterile feedstock. Subsequent generations were grown from a mixture of the previous generation object, reground to granularity without sterilization, and further unsterilized, non-inoculated feedstock. Primary inoculum was generated by mixing 30 g *Ganoderma* sp. spawn, grown on white millet, 600 g hemp sterilized in a pressure cooker, 24 g $CaSO_4$, 1,100 ml water and 42 g clear flour, then placing the mixture in sterile polyethylene vented bags and allowing it to grow for 5 days at 24 °C. For the material characterization shown in Supplementary Table 1, this inoculum was then reduced back to particulate and an additional 84 g flour was added. This material was then packed into plastic moulds and grown for an additional 5 days to form test objects. The test objects were removed from their moulds and desiccated in a convection oven prior to testing. For all other experiments, 'first-generation' objects were generated by mixing 35 g dried raw, unsterile hemp substrate with 100 g primary inoculum (about equal volumes given the water content of the primary inoculum), 4 g $CaSO_4$, 14 g flour and 65 ml water to homogeneity in a clean plastic tub, then placing the granular material in moulds, loosely covering with foil and growing for 5 days at room temperature. The objects were then desiccated to <10% moisture content, measured using a Mettler Toledo HB43-S Classic Plus moisture analyser, and then used or reground as inoculum for subsequent generations (Gen2+) of objects. For these Gen2+ objects, 35 g hemp substrate was mixed with 35 g dried and reground first-generation biocomposite, along with 4 g $CaSO_4$, 14 g flour and 130 ml water, then moulded, grown and desiccated as before. For block fusion, the objects were demoulded after 5 days as usual, then placed in contact and allowed to further grow during the early desiccation period to fuse. For the large, fused-block arch, individual subunits were demoulded, placed on a concave wooden form until desiccated and fused, then the arch was flipped. Hinges were embedded into the material either by simply lining the desired mould junctions with FlaxCraft Hemp Fiber Mat, 750 grams per square meter weight before adding biocomposite prior to growth, if the hinge was desired on the 'bottom' face of the object, or by laying the matting on the top of the mould during biocomposite growth. Flat-pack slot-together moulds were constructed using laser-cut 0.023 caliper Badger Paperboard Plain sheet with poly-coating. Blocks created in slot-together moulds were grown using the typical recipe, but covered loosely with a plastic sheet during the growth phase to maintain a humidity of at least 60% and allow passive aeration. To test block repair, blocks were grown for 5 days, then wounded either by tearing down the middle or manually removing material to form a hole. Torn blocks were simply placed back into their moulds, the two halves in contact, then grown either in ambient laboratory conditions or in controlled 60% humidity. Holes were backfilled with first-generation material, then covered with plastic wrap to retain moisture and grown for an additional 7 days. Strength testing was accomplished by ASTM (D1621-16, C165-07 and C203 tests) on Instron 4411 and 3345 universal testing machines. Material ergosterol was measured by standard methanol extraction and HPLC quantification with methanol as the mobile phase on a RoC C_{18} 5 µm 100 mm × 4.6 mm column and 280 nm detection on an Agilent Technologies Series 1100 HPLC instrument. The ergosterol peak was measured at approximately 6.8–7 min. The percentage fungal mass was calculated as:

$$\text{Ergosterol mass (mg)} = (\text{integrated peak} \times 12.5\ \text{ml extraction volume})$$

$$\text{Fungal mass per sample mass} = 0.2516 \times \text{ergosterol mass} - 0.0007$$

$$\text{Fungal mass percentage} = \text{fungal mass per sample mass/dry sample mass} \times 100$$

The pH of the material was measured using a Hanna HI 99121 Direct Soil pH meter. Flat-pack slot-together moulds were designed and biomaterial objects simulated by finite element analysis using Autodesk Fusion 360.

16S rRNA, ITS and whole genome sequencing and data analysis. DNA was extracted following a standard protocol using a Qiagen MagAttract PowerMicrobiome extraction kit. Briefly, 1 g samples were added to an Axygen 2-ml-deep 96-well plate along with 200 ml BioSpec zirconia silica beads and 750 µl lysis buffer (9 ml Tris-HCl, pH 7.5, 9 ml of 0.5 M EDTA, pH 8.0, 11.25 ml of 10% SDS, 22.5 ml Qiagen lysis reagent and 38.25 ml nuclease-free water), covered with an Axygen silicone sealing mat, then disrupted using a BioSpec 1001 96-cell bead-beader for 2 min 30 s at room temperature, followed by cooling for 5 min. This process was repeated another three times. The plates were then centrifuged at 4,300*g* for 5 min at 4 °C, and 200 µl supernatant was transferred to a 96-well V-bottom plate. Lysis was halted using 35 µl Qiagen inhibitor removal solution, then the plates were centrifuged at 4,300*g* for 5 min and 100 µl supernatant was transferred to a round-bottom 96-well plate without disturbing the protein pellet. A robotic handler (Biomek 4000) was used for magnetic bead purification, and the resultant DNA was quantified on a Tecan plate reader using SYBR stain according to the manufacturer's instructions. Samples were pooled at equal molarity and the pools were run on 2% agarose gel. The bands at 390 bp were cut out and the DNA was purified with a Promega Wizard SV gel and PCR cleanup system. Size-selected pools were quantified by Qubit and finally diluted to 10 pM and sequenced with a 20% spike-in of a PhiX control using an Illumina Miseq V2 sequencing kit.

The V4 region of the bacterial 16S rRNA gene and the ITS1 region of the fungal rRNA region were sequenced using a previously established pipeline[32] (the primers are detailed in Supplementary Table 7). Briefly, PCR amplicons were generated from each sample using primers compatible with direct amplicon sequencing on the Illumina MiSeq sequencing platform. After PCR amplification, samples were pooled and the ~390 bp 16S and ~400 bp ITS amplicon bands were gel-purified. The 16S sequences were processed using the standard DADA2 pipeline[37] with a truncation length of 150 bp for forward and reverse reads, max$N$ = 0, truncation at a quality Q-score of 2 and a maximum expected error of 1 for all reads. Bimeras were removed and these sequences were taxonomically identified using the default Ribosomal Database Project (RDP) classifier and the SILVA database (version 132) (ref. [38]). Fungal sequences were processed using the DADA2 ITS workflow (https://benjjneb.github.io/dada2/ITS_workflow.html) with sequencing adapters removed and then filtered using the parameters max$N$ = 0, maximum expected errors of 2, read truncation quality of 2 and minimum length of 50 bp. Bimeras were removed and the sequences were identified using the RDP classifier and the UNITE database (release 1/12/2017) (ref. [39]). Bar plots were generated using the plot_bar function in phyloseq, and principal component plots were generated using the ordinate and plot_ordination functions using the Bray–Curtis dissimilarity. For heat maps, reads were merged, filtered and clustered to OTUs using USEARCH (ref. [40]) and DADA2, then classified using RDP (ref. [41]) and phyloseq (ref. [42]). The heat maps were then generated using Matplotlib and ggplot2. For absolute abundance measurements by amplicon sequencing, a standardized concentration per mass of a normalization bacterial strain not expected to be present in any sample, *Sporosarcina pasteurii* (ATCC 11859), was added to each sample prior to DNA isolation. Sample reads were normalized to reads resulting from this strain to provide absolute bacterial measurements[32].

Strain isolation, cultivation and characterization. Bacterial strains were isolated from hemp feedstocks by several methods that involved washing with mechanical disruption. In all cases, raw hemp feedstock was suspended in sterile PBS, and then subjected to mechanical disruption to free attached bacteria and spores using two approaches. For the immediate isolation approach, 5-mm glass beads were added to the hemp suspension in 50-ml Falcon tubes and vortexed for either 30 s or 5 min. For the extended isolation approach, similar pulse-vortexed hemp suspensions were left nutating overnight at room temperature before serial plating. Following cell liberation (immediate isolation) or recovery (extended isolation), cell suspensions were gently spun down and supernatant serially diluted onto 2×YT agar plates and grown overnight at 30 °C to obtain single colonies, which were picked and restreaked to obtain clonal isolates. Isolates were grown overnight in liquid 2×YT at 30 °C, then identified by PCR of the full-length 16S amplicon and Sanger sequencing. The 16S sequences were analysed by Basic Local Alignment Search Tool (BLAST) against the National Center for Biotechnology Information (NCBI) 16S sequence database using the SILVA web server (arb-silva.de)[43]. The generated trees were visualized using the Interactive Tree of Life (itol.embl.de)[44]. In all, 33 colonies were characterized, belonging mostly to the *Bacillus* and *Pantoea* groups (Extended Data Fig. 5). Interestingly, the colonies isolated from the direct resuspension of the feedstock almost exclusively belonged to *Bacillus*, known spore-forming *Firmicutes* prevalent in soil and agricultural associated substrates. On the other hand, colonies from overnight suspension of the feedstock and subsequent plating yielded mostly *Enterobacteria* of the *Pantoea* group. From this cohort, we chose the isolate (ID30) most closely related to *P. agglomerans* for further study. *P. agglomerans* ELM1 was subsequently cultivated using LB media at 30 °C unless stated otherwise.

Antibiotic sensitivity tests were performed on *P. agglomerans* ELM1 using Liofilchem minimum inhibitory concentration (MIC) test strips according to the manufacturer's instructions on LB agar and in liquid culture using 0.1×, 0.5×, 1× and 2× typical antibiotic working concentrations (WC; carbenicillin, WC = 50 µg ml^{-1}; kanamycin, WC = 100 µg ml^{-1}; tetracycline, WC = 10 µg ml^{-1}; chloramphenicol, WC = 25 µg ml^{-1}; gentamycin, WC = 10 µg ml^{-1}; spectinomycin, WC = 50 µg ml^{-1}) using a BioTek Synergy H1 plate reader in 96-well-plate format.

Carbon source utilization was tested in M9 minimal medium at 5 mM carbon source concentration, except for the poly(ethylene glycol) PEG8000, which was tested at 1% vol/vol. A saturated overnight culture of *P. agglomerans* was washed three times in sterile PBS, then diluted 1:1,000 and 1 µl was used to inoculate 100 µl of sterile filtered M9–carbon source medium in a 96-well plate, which was then measured in a BioTek Synergy H1 plate reader with shaking (triplicate optical density at 600 nm (OD600) versus individual carbon source blanks). Boiled hemp medium was prepared by suspending about 10 g hemp stover in just enough water to allow magnetic stirring, then boiling on a hot plate for 15 min, removing the wet hemp using cheesecloth and sterile filtering.

Transformation, conjugation and transposon integration protocols. The plasmids used or generated in this study are listed in Supplementary Table 6. Plasmids were transformed into *P. agglomerans* using a standard bacterial electroporation protocol. Briefly, an overnight cell culture was diluted 1:1,000 and allowed to grow to the mid-log phase (OD600 = 0.4–6). The cells were then washed, pelleted and resuspended in sterile ice-cold water in equal volumes three times. In the last wash, the cell pellets were resuspended in 100 µl water per millimetre of prewashed cells and either snap-frozen in liquid nitrogen or used directly for electroporation. A BioRad MicroPulser electroporator with a 0.1-cm gap cuvette was used to deliver a 1.8 kV pulse. The cells were immediately recovered in 1 ml super optimal broth with catabolite repression medium (SOC) at 30 °C for at least 1 h before plating on agar. Plasmid copy numbers were measured by quantitative PCR of 1 µl of saturated overnight cultures with pUC19-Spec (PMB1 derivative ori), pQE (ColE1 ori), pBR322 (PMB1 ori), pACYC (p15a ori) or pSZ24 (SC101 ori) using KAPA Sybr Fast with ori-specific primers or genomic *lacZ* and *elgF* primers for normalization (Supplementary Table 7) according to the manufacturer's protocol. The transformation efficiency with electroporation was quantified by using a tenfold molar excess of freshly prepared electrocompetent *P. agglomerans* cells with various amounts of pUC19-spec plasmids in 1 µl, recovered for 1 h in SOC and serially diluted and plated for colony formation unit counting. The conjugation efficiency was evaluated using a diaminopimelic acid (DAP)-deficient *E. coli* donor strain[45] containing an RK2 conjugative plasmid with a Tet marker. Mid-log phase cultures of *E. coli* donor and *P. agglomerans* recipients were diluted to OD600 ≈ 0.1, mixed in a donor-to-recipient ratio of 1:9, 1:1 or 9:1 in a total of 1 ml, then spun down, resuspended in a minimum amount of PBS to allow pipetting, spotted onto agar plates and allowed to dry and conjugate for 1 h at 30 °C. After that time, the cells were scraped into 300 µl LB medium and serially diluted and plated onto Tet+, DAP– plates to select for successful transconjugants and onto Tet+, DAP+ plates to quantify the number of donor cells. The efficiency was evaluated as successful transconjugants per donor at a given donor/recipient ratio. Genomic integration by Tn*7* transposition was accomplished using the pGRG36 system[30], with a slightly modified protocol. Briefly, a variant of the pGRG36 plasmid was constructed carrying an eGFP:Kan cassette, then transformed into *P. agglomerans* cells, grown overnight in liquid culture without selection or induction to allow insertion, then plated on Kan+ media. Five colonies from the resultant plates were then cured overnight in liquid culture at 37 °C, then plated onto Kan plates for a further 3 days before being evaluated for successful integration by colony PCR with primers flanking the Tn*7* integration site in the *P. agglomerans* ELM1 genome (the primers are listed in Supplementary Table 7). Antibiotic resistance plasmids with successful selection in *P. agglomerans* ELM1 are listed in Supplementary Table 6.

Genome sequencing and characterization. The *P. agglomerans* ELM1 genome was sequenced by a combination of Illumina short-read and Pacbio long-read sequencing. The Illumina sequencing library was generated using the Nextera XT DNA Library Preparation Kit (Illumina) and sequencing was performed on a MiSeq instrument using 2 × 151 bp paired-end sequencing and v2 chemistry to a depth of ~27x. Long-read PacBio sequencing was performed using SNPSaurus (www.snpsaurus.com). The genome was assembled using Unicycler[46] in hybrid mode with default settings, and annotation was performed with Prokka[47] using the default settings. The nearest neighbour was determined by BLAST against RefSeq genomes, and then the average nucleotide identity (ANI) was determined using the EZBioCloud ANI server (ezbiocloud.net/tools/ani)[48]. Biosynthetic gene clusters were identified using the antiSMASH web server (https://antismash.secondarymetabolites.org) using the default strictness and all extra features[49]. CAZymes were identified using the dbCAN2 web server (https://bcb.unl.edu/dbcan2)[50] and filtered to only include glycoside hydrolase (GH) and auxiliary activities (AA) class CAZymes, which were detected using all three identification methods (HMMER, Hotpep and DIAMOND), then manually cross-referenced against the Prokka annotations. A non-systematic manual search in the Prokka output protein list for terms such as 'laccase' and 'peroxidase' resulted in an additional two hits. Putative antibiotic genes were identified using the CARD online web portal (card.mcmaster.ca/analyze) using both the Resistance Gene Identifier (RGI) and BLAST (70% identity cut-off) methods[51]. A further non-systematic manual search in the Prokka annotations for 'lactam' and 'icin' resulted in an additional five hits (Supplementary Table 2).

Promoter strength measurement and flow cytometry. A set of promoters derived from natural genomes described previously[52] were used to drive a *gfp* reporter in a p15a plasmid backbone (Supplementary Table 8). The promoter activity was characterized in *P. agglomerans* ELM1 using a BioTek Synergy H1 plate reader (GFP fluorescence versus OD600) and a Guava Easycyte 5 benchtop flow cytometer. For flow cytometric measurements, events were gated on forward and side scatter to match a diluted culture of wild-type *P. agglomerans* to exclude multiple cell events. The promoters were Sanger-sequenced to verify the regulatory sequence (the primers are listed in Supplementary Table 7).

Violacein and carotenoid extraction and characterization. *P. agglomerans* cells carrying the synthetic pathways were grown overnight in 30 ml LB–Kan in at 30 °C with 250 r.p.m. shaking. The cells were pelleted by centrifugation, resuspended and lysed in 3 ml ethanol with vortexing and bath sonication. The intensely coloured supernatants were separated from the almost white cell debris by centrifugation and passed through a 0.22-µm syringe filter without further purification. Aliquots of the extracts were diluted with an equal volume of methanol and subjected to liquid chromatography mass spectrometry analysis. Reversed-phase HPLC was performed with a C_{18} column on an Agilent 1260 Infinity II LC System. The mobile phase was switched linearly from 90:10 to 5:95 water–acetonitrile in 18 min. The fractions were further ionized by electrospray and analysed with a tandemly connected mass spectrometer (Agilent 6420 Triple Quadrupole). For comparison, a standard solution of 1 µg ml^{-1} violacein in 50:50 ethanol–methanol was prepared from commercially purchased violacein (Sigma Aldrich, V9389).

In-material expression. *P. agglomerans* cells carrying pCHR896, which constitutively expresses mCherry under a RiboJ insulated BBaJ23100 promoter, were incorporated into blocks generated using a modified version of the standard first-generation protocol. Briefly, 1 l of overnight cell culture was concentrated by centrifugation and resuspension in LB medium with 50 µg ml^{-1} kanamycin. This cell suspension was used to substitute 40% of the water in the standard first-generation protocol, which resulted in an inoculation density of about 10^9 *P. agglomerans* cells per gww of unmoulded biocomposite. Next, 5.08 × 5.08 × 5.08 cm biomaterial blocks were grown in lidded silicone ice-cube trays for 6 days at room temperature, then broken open to expose the block interior and imaged using a BioRad Chemidoc imager with green epi illumination and a 605/50 nm bandpass filter. Violacein-functionalized blocks were constructed similarly, but carrying the pNM175 plasmid at a loading rate of 10^9 *P. agglomerans* cells per gww.

Signal propagation system construction and testing. The AHL-producing plasmid pCHR191 was generated by cloning the *Rhizobium leguminosarum* AHL synthase *cinI*, driven by a BBaJ23100 constitutive promoter, into a p15A ori backbone with a kanamycin marker. The construct produces the specific AHL *N*-tetradecanoyl-L-homoserine lactone. The AHL-responsive plasmid pCHR91 was generated by cloning *cinR*, the *R. leguminosarum* quorum-sensing transcriptional activator analogue of *luxR*, driven by a BBaJ23100 promoter, as well as mCherry under the control of *R. leguminosarum cinR*-responsive promoter pCin, into a p15A ori backbone with a Kan marker. Plasmid maps are included in the Supplementary Data files.

To test the basic quorum molecule sensing of the bulk material, 5.08 × 5.08 × 5.08 cm biomaterial blocks with 10^9 *P. agglomerans* per gww carrying the AHL-responsive pCHR91 plasmid were grown as above with or without 10 µM AHL included in the water in the block recipe. To test cell–cell communication within the biocomposite material, two large (22.86 × 33.02 cm) biocomposite panels were inoculated and grown using the same protocol described above with *P. agglomerans* carrying ALH-responsive pCHR91 plasmid. A third large panel was left uninoculated as a control. Two small 5.08 × 5.08 × 5.08 cm biomaterial cubes inoculated with *P. agglomerans* carrying AHL-producing pCHR191 were also generated. All the panels and cubes were grown separately over 7 days. Following growth, the cubes were demoulded and hydrated by placing each into a 5-l shaker flask along with 150 ml LB–Kan (50 µg ml^{-1}) and incubated for 16 h at 30 °C with 75 r.p.m. gentle shaking. The three large panels were left in their moulds, 50 ml LB–Kan was added directly to the material and similarly shaken and incubated. After incubation, one small AHL-producing cube was placed on one larger AHL-responsive panel to test material responsiveness. Another small cube was placed on the uninoculated panel as a negative control. The final large panel was left without a small sender cube as another negative control. An additional 30 ml LB–Kan was then added to each, and then the cubes/panels were covered with foil to retain moisture and incubated again for 16 h at 30 °C with 75 r.p.m. shaking. Following the second incubation, the cubes/panels were imaged with the Chemidoc imager with a 605/50 nm filter.

For the feed-forward spatial signal propagation system, AHL-producer plasmid pCHR661 was generated by cloning a *cinI*-mCherry operon, driven by a BBaJ23100 constitutive promoter, into a p15a/Kan backbone. AHL-feed-forward-responsive plasmid pCHR770 was generated by cloning the same *cinI*-mCherry operon into a p15a/Kan backbone, but driven by a pCin AHL-responsive promoter. In addition, the *R. leguminosarum cinR* quorum-sensing transcriptional activator and the *Bacillus thuringiensis* AHL lactonase *aiiA* were constitutively expressed under the same promoter. This plasmid was manually tuned to maximize sensitivity and minimize autoactivation. To tune the plasmid, first, a degenerate RBS sequence (TAYACTGTAGAGTYWCASRACC) was cloned upstream of the *aiiA* gene, the vector transformed into *P. agglomerans* and then six randomly picked colonies were tested for sensitivity and autoactivation. Two rows of 2.5 nl volume pCHR770-variant-carrying *P. agglomerans* colonies were spotted onto agar plates at a spacing of 0.5 mm using an Echo 550 liquid handler. One of the rows of colonies was activated by spotting an additional colony carrying the AHL-producing pCHR191 at one end of the row at the same spacing. The other row was left without an activating colony to control for autoactivation. The plate was incubated overnight at 30 °C and then imaged for mCherry fluorescence on a Chemidoc imager. The plasmid variant with no autoactivation but the highest signal propagation down the line of colonies from the AHL-producing colony was

selected for further optimization with a *cinI* RBS library. The same degenerate RBS was cloned in front of the *cinI* gene, and six colonies were similarly screened for maximal sensitivity without autoactivation. The final candidate was tested using a 14×14 2D array of Echo-spotted colonies at a spacing of 2.5 mm. For activation, one corner colony was omitted and replaced by either a colony producing AHL or left empty as a negative control, and then the colonies were grown overnight at 30 °C and similarly imaged using ChemiDoc. Initial testing of the propagator strain responsiveness in blocks was performed at a loading rate of 10^9 cells per gww of pCHR770-carrying *P. agglomerans* by dripping 0.5 ml of 100 µM AHL solution onto the surface of newly packed, pregrowth 5.08×5.08×5.08 cm biomaterial blocks, and then growing and imaging as before.

To explore the critical parameters of this system a reaction-diffusion simulation of the signal propagation system was performed in silico. An explicit (forward Eular) finite difference method was applied to a 2D square lattice with a 0.1-mm grid size and a temporal step size of 0.001 h. Colonies were approximated as circles with a diameter of 1 mm, which is about the medium size during the growth period. The diffusivity of the AHL was assumed to be 2 $mm^2 h^{-1}$, and a background degradation rate of 0.2 h^{-1} was also used. Within the 'colonies', the quorum-sensitive promoter was modelled using Hill functions with a fold change of 100 and a Hill coefficient of 2. AHL synthase proteins were assumed to have an inactivation half-life of 8 h. Fluorescent protein mCherry was assumed to be stable. To account for the initial exponential growth of cell number and the gradual decline of metabolic activity (synthase expression) as more cells enter the stationary phase, an activity function was used for all colonies. The protein synthesis capacity of a colony is proportional to the activity in the growth stage, and the activation/repression of inducible promoter further determines the protein synthesis rate. The activity was modelled as the product of two logistic functions at time (t), resulting in an initial exponential increase, a plateau and a more gradual decline:

$$\text{Activity}\,(t) = \frac{\frac{1}{1+e^{8-t}}}{1+e^{(t-34)/4}}$$

Reporting Summary. Further information on research design is available in the Nature Research Reporting Summary linked to this article.

Data availability

The sequencing data generated for this study are deposited in the NCBI SRA, accession number PRJNA673748. Metagenomic samples were classified against the SILVA database v.132 and RDP Classifier training set 17 (16S) and the UNITE database vl.12.17 (ITS). Source data are provided with this paper.

Code availability

The code used in the development of the signal propagation system design described in Fig. 4 is available at https://github.com/wanglabcumc/FungalBiocomposites.

References

37. Callahan, B. J. et al. DADA2: high-resolution sample inference from Illumina amplicon data. *Nat. Methods* **13**, 581–583 (2016).
38. Callahan, B. Silva taxonomic training data formatted for DADA2. Silva v.132. Zenodo https://doi.org/10.5281/zenodo.1172783 (2018).
39. Nilsson, R. H. et al. The UNITE database for molecular identification of fungi: handling dark taxa and parallel taxonomic classifications. *Nucleic Acids Res.* **47**, D259–D264 (2019).
40. Edgar, R. C. Search and clustering orders of magnitude faster than BLAST. *Bioinformatics* **26**, 2460–2461 (2010).
41. Wang, Q., Garrity, G. M., Tiedje, J. M. & Cole, J. R. Naive Bayesian classifier for rapid assignment of rRNA sequences into the new bacterial taxonomy. *Appl. Environ. Microbiol.* **73**, 5261–5267 (2007).
42. McMurdie, P. J. & Holmes, S. phyloseq: an R package for reproducible interactive analysis and graphics of microbiome census data. *PLoS ONE* **8**, e61217 (2013).
43. Quast, C. et al. The SILVA ribosomal RNA gene database project: improved data processing and web-based tools. *Nucleic Acids Res.* **41**, D590–D596 (2013).
44. Letunic, I. & Bork, P. Interactive Tree Of Life (iTOL) v4: recent updates and new developments. *Nucleic Acids Res.* **47**, W256–W259 (2019).
45. Ronda, C., Chen, S. P., Cabral, V., Yaung, S. J. & Wang, H. H. Metagenomic engineering of the mammalian gut microbiome in situ. *Nat. Methods* **16**, 167–170 (2019).
46. Wick, R. R., Judd, L. M., Gorrie, C. L. & Holt, K. E. Unicycler: resolving bacterial genome assemblies from short and long sequencing reads. *PLoS Comput. Biol.* **13**, e1005595 (2017).
47. Seemann, T. Prokka: rapid prokaryotic genome annotation. *Bioinformatics* **30**, 2068–2069 (2014).
48. Yoon, S. H., Ha, S. M., Lim, J., Kwon, S. & Chun, J. A large-scale evaluation of algorithms to calculate average nucleotide identity. *Ant. Van Leeuw.* **110**, 1281–1286 (2017).
49. Blin, K. et al. The antiSMASH database version 2: a comprehensive resource on secondary metabolite biosynthetic gene clusters. *Nucleic Acids Res.* **47**, D625–D630 (2019).
50. Zhang, H. et al. dbCAN2: a meta server for automated carbohydrate-active enzyme annotation. *Nucleic Acids Res.* **46**, W95–W101 (2018).
51. Alcock, B. P. et al. CARD 2020: antibiotic resistome surveillance with the comprehensive antibiotic resistance database. *Nucleic Acids Res.* **48**, D517–D525 (2020).
52. Johns, N. I. et al. Metagenomic mining of regulatory elements enables programmable species-selective gene expression. *Nat. Methods* **15**, 323–329 (2018).

Acknowledgements

We thank the members of Wang Lab for comments and discussion on this work and manuscript. This work is supported by DARPA (HR0011-17-C-0068, W911NF-17-2-0077) and NSF (CCF-1807575). H.H.W. acknowledges additional funding from NSF (MCB-2032259, MCB-2025515, MCB-1453219), NIH (1R01AI132403, 1R01DK118044) and the Burroughs Wellcome Fund (PATH1016691). R.M.M. thanks personal support from X. Weng and financial support from the Dean's Fellowship from the Graduate School of Arts and Sciences of Columbia University. M.R. is supported by an NSF Graduate Research Fellowship (DGE-1644869).

Author contributions

R.M.M., M.L, C.V., D.S. and H.H.W. developed the initial concept. R.M.M., M.L., N.M., T.S., D.M., H.C., A.K., M. Richardson and M. Reitman performed experiments and analysed the results. M. Richardson, R.M.M. and C.M. analysed the metagenomic and whole genome sequencing data. The overall project was supervised by C.V., D.S. and H.H.W. The manuscript was drafted by R.M.M. and H.H.W. with input from all authors.

Competing interests

M.L., M. Reitman and D.S. are employees of Ecovative Design, at the time of study. The authors declare no additional competing interests.

Additional information

Extended data is available for this paper at https://doi.org/10.1038/s41563-021-01123-y.

Supplementary information The online version contains supplementary material available at https://doi.org/10.1038/s41563-021-01123-y.

Correspondence and requests for materials should be addressed to Damen Schaak or Harris H. Wang.

Peer review information *Nature Materials* thanks the anonymous reviewers for their contribution to the peer review of this work.

Reprints and permissions information is available at www.nature.com/reprints.

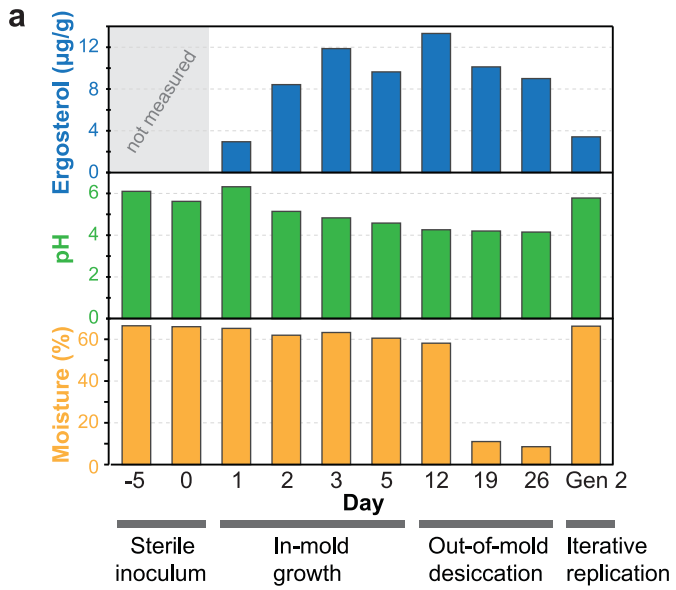

Extended Data Fig. 1 | Growth characteristics of *Ganoderma sp.* in the living biocomposite. (**a**) The level of moisture, pH, and ergosterol, which is a measure of fungal biomass, was quantified over the course of a full cycle of biomaterial generation and subsequent iterative replication in Generation 2 of reground biomaterial.

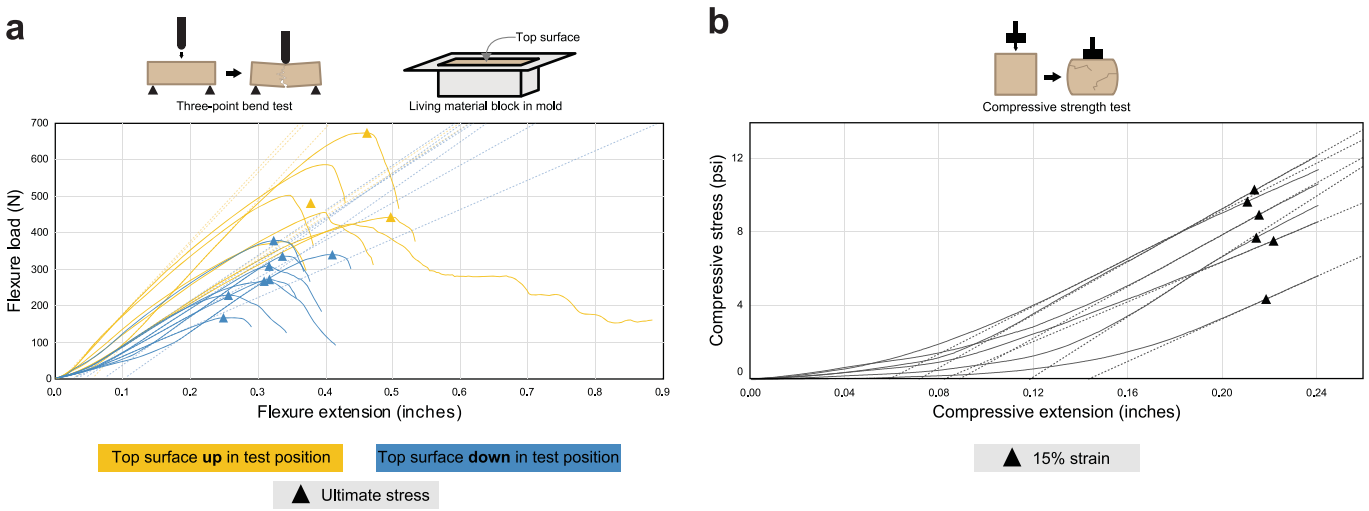

Extended Data Fig. 2 | Representative strength characterization for fungal biocomposites. (**a**) Representative three-point bend test results for living material blocks in two orientations. Note the anisotropy in the results, presumably due to differences in fungal growth due to aeration or other factors at the top of the block mold, even when lidded. (**b**) Representative compressive strength test results for living material blocks.

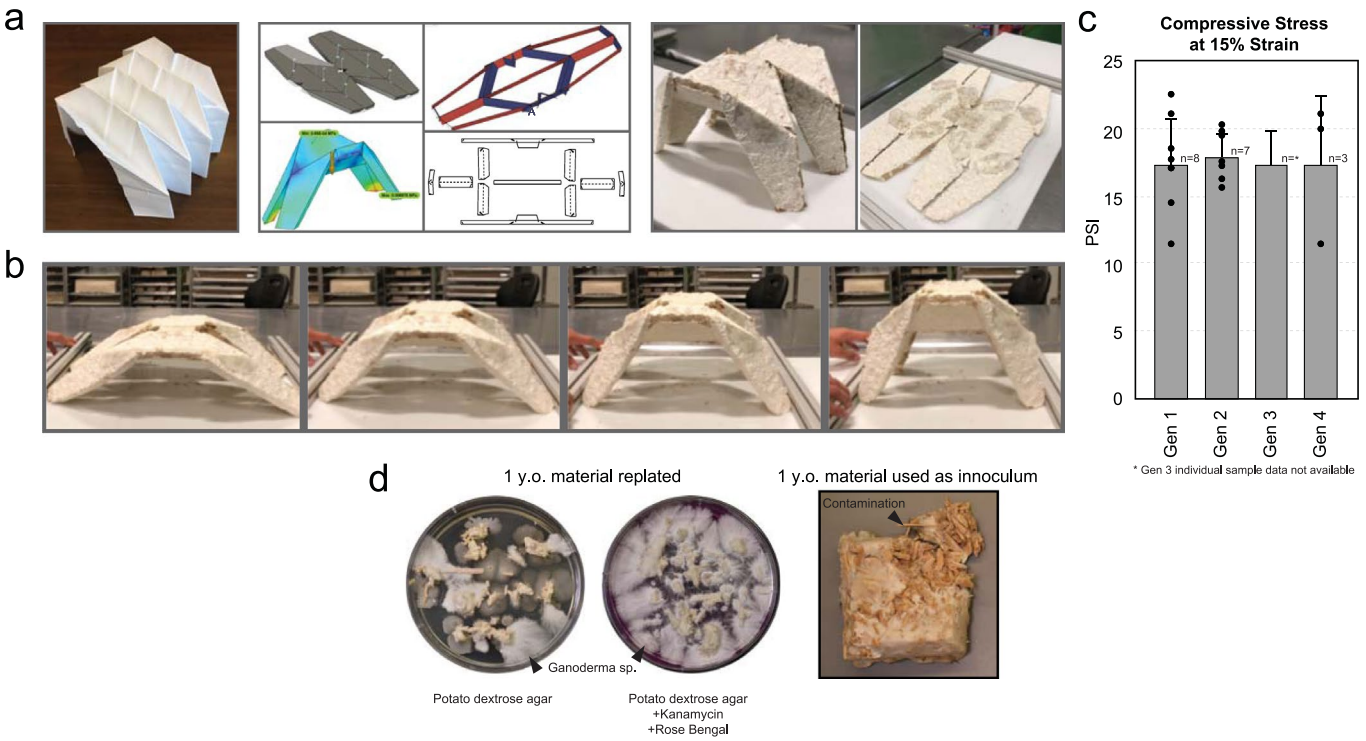

Extended Data Fig. 3 | Foldable biocomposite designs and generation of pop-up structures. (**a**) The design process for complex origami-inspired structures, beginning with conceptual models, followed by *in silico* modeling, simulation, layout, and fabrication to produce a final object. An arch design is first grown on a flat surface using flat-pack molds along with the appropriate connecting joints and folding edges on the top and bottom surfaces using flexible matting. (**b**) The arch is kinematically erected via a pop-up assembly protocol, and the joints are allowed to naturally fuse, thus stabilizing the arch structure into its final designed form. (**c**) Compressive strength of hemp-grown fungal biocomposite over four generations. Bar graphs shows the mean of and error bars show the standard deviation (SD). (**d**) Replated and regrown living material after a year of ambient desiccation. The *Ganoderma sp.* is still viable, and easily recultivated, especially with kanamycin antibiotics and Rose Bengal as a mold suppressor. Blocks grown using this material as an inoculum, however, are prone to contamination.

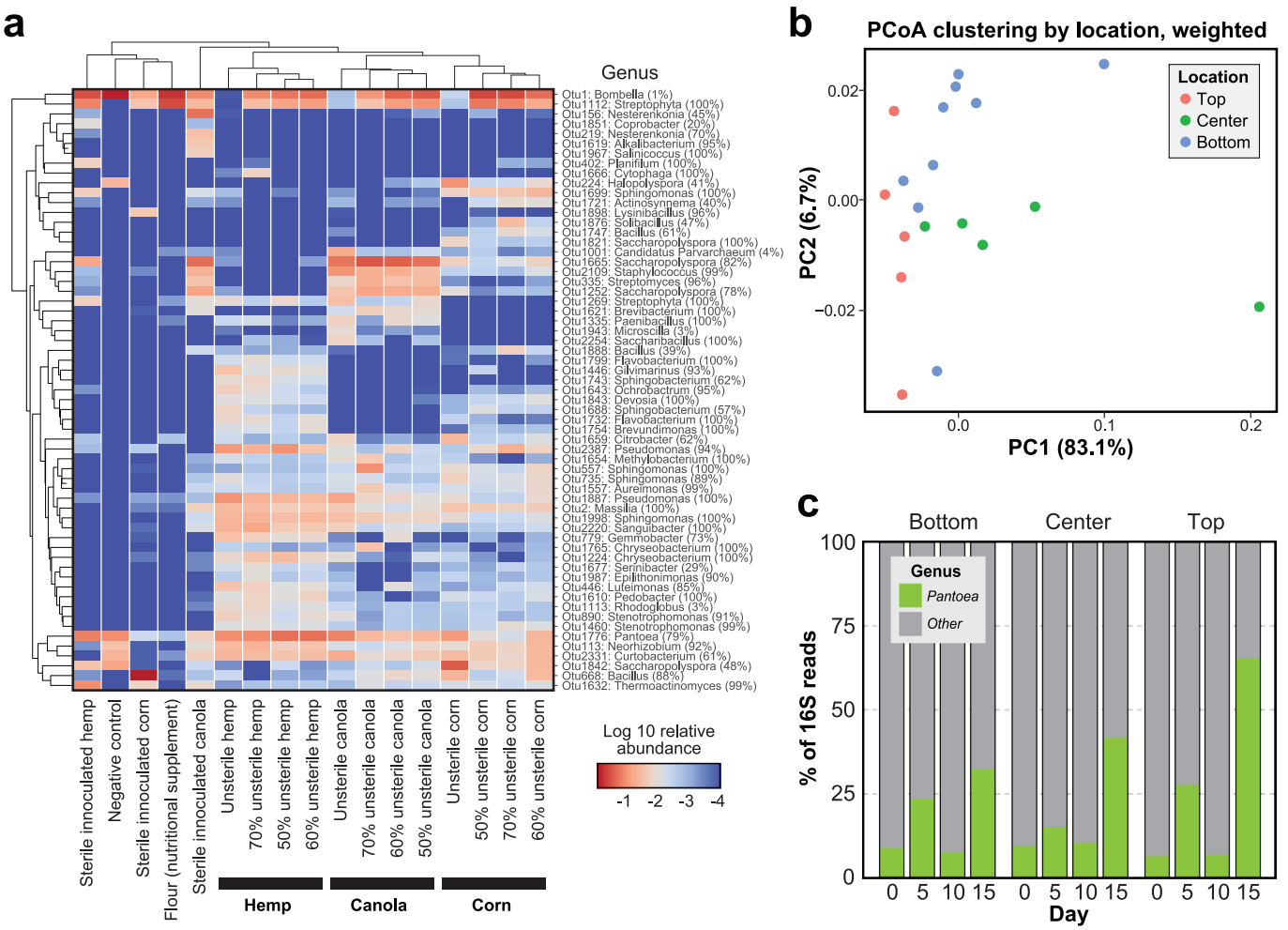

Extended Data Fig. 4 | Microbiome characteristics of the living biocomposite. Microbiome characteristics of the living biocomposite (a) Clustered heatmap of the bacterial abundance in biomaterial grown using different feedstocks and at different inoculation ratios (% sterile inoculum to % unsterile raw feedstock). Heatmap is in log10 scale in relative bacterial abundance. (b) Bacterial microbiome in a grown hemp block sampled at different spatial locations. At least 5 replicates per sampling location were analyzed (n = 5). (c) Analysis of 16 S reads at each spatially sampled location of a growing hemp block over 15-days, showing reproducible dominance of *Pantoea* spp.

a

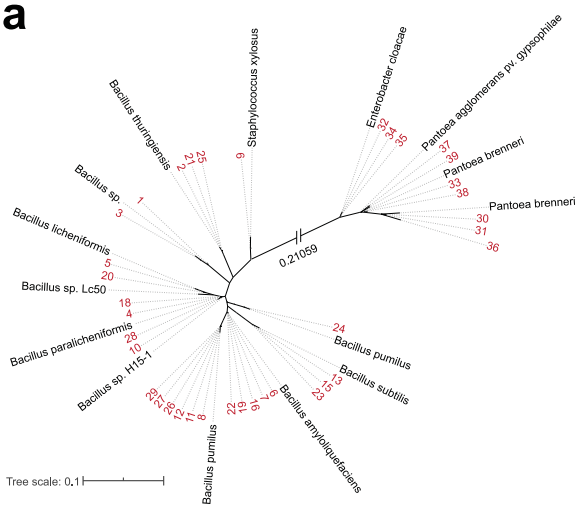

b

Isolate ID#	Species class. by refseq genomes BLAST	Isolation strategy: Immediate	Isolation strategy: Overnight
1, 3	Bacillus megaterium	■	
2, 21, 22, 25	Bacillus cereus group	■	■
4, 5, 20, 28	Bacillus licheniformis	■	■
6, 19, 23	Bacillus subtilis	■	
7, 13, 15, 16	Bacillus amyloliquefaciens group	■	
8	Bacillus safensis	■	
9	Staphylococcus xylosus	■	
10, 18	Bacillus paralicheniformis	■	
11	Bacillus pumilus	■	
12, 24, 26, 27, 29	Bacillus altitudinis	■	■
30, 31, 33, 36, 37, 38, 39	Pantoea agglomerans		■
32, 34, 35	Enterobacter cloacae group		■

Extended Data Fig. 5 | Strain isolation from hemp feedstock. (**a**) Unrooted tree of 33 isolates from hemp feedstock, mapped to the SILVA 16 S database. (**b**) Table of isolates and closest BLAST match against the NCBI 16S database. Isolates were either plated immediately from PBS-washed feedstock supernatant or allowed to wash and recover overnight before plating, which enriched for *Pantoea spp*. Note: Isolate ID #30 is annotated as *Pantoea ananatis* by NCBI 16S database, but was subsequently confirmed to be *P. agglomerans* and designated as *P. agglomerans* ELM1 throughout the study.

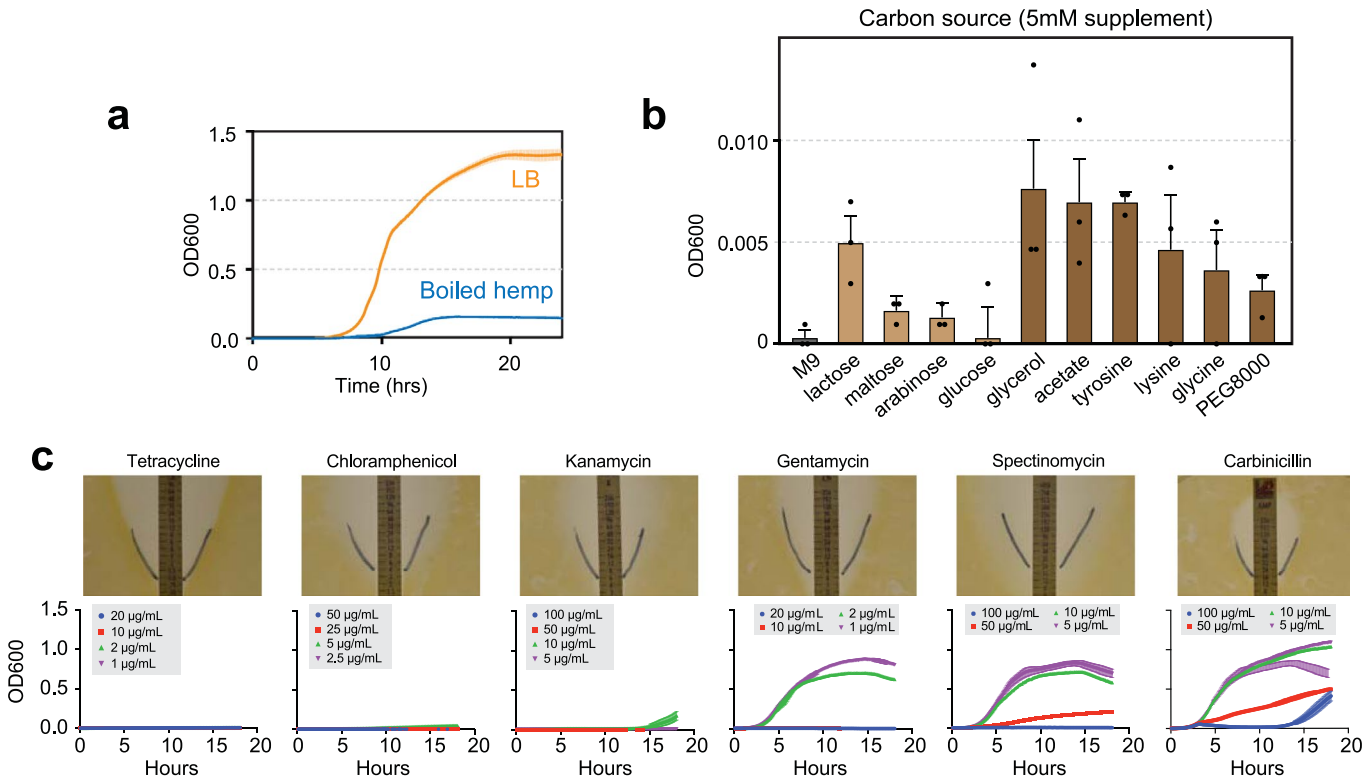

Extended Data Fig. 6 | Growth characteristics of *P. agglomerans* ELM1. (**a**) *P. agglomerans* ELM1 growth on standard LB rich media at 30 °C, as well as on a boiled hemp media derived from the same material feedstock from which the strain was isolated. Error bars show standard error of the mean (SEM) of three biological replicates (n = 3). (**b**) OD600 of *P. agglomerans* ELM1 in M9 minimal media on a number of carbon sources showing modest growth after 24 hours at 30 °C. Error bars show SEM. (**c**) Antibiotic susceptibility of *P. agglomerans* ELM1 (top) and their liquid growth profiles at different antibiotic concentrations (bottom). Error bars show SEM of three biological replicates (n = 3).

a

Pantoea agglomerans ELM1 **genome**	
Coverage:	27x Ilumina, 237x Pacbio
Size:	4.8 Mbp
GC content:	55%
Plasmids:	2
CDS:	4413

GC content
(+) CDS
(-) CDS

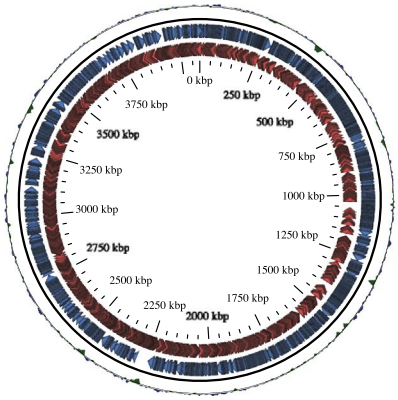

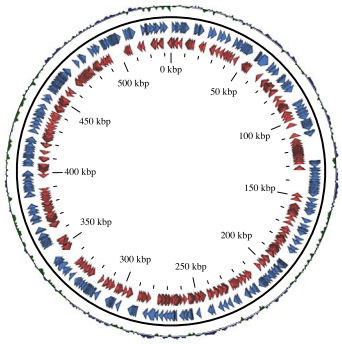

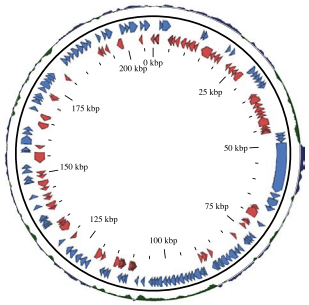

Chromosome	
Size:	4,083,589 bp
CDS:	3,712 CDS
Homology:	*Pantoea agglomerans* L15 (3.572e5) *Pantoea agglomerans* CFSAN047153 (3.162e5) *Pantoea agglomerans* CFSAN047154 (3.162e5)

Plasmid 1	
Size:	534,623 bp
CDS:	513 CDS
Homology:	*P. agg.* L15 plasmid pPagL15_1 (1.492e5) *P. agg.* TH81 plasmid unnamed1(1.375e5) *P. agg.* CFSAN047153 plasmid pCFSAN047153_1 (99557)

Plasmid 2	
Size:	207,673 bp
CDS:	179 CDS
Homology:	*P. agg.* CFSAN047153 plasmid pCFSAN047153_2 (1.057e5) *P. agg.* CFSAN047154 plasmid pCFSAN047154_2 (1.057e5) *P. agg.* TH81 plasmid unnamed2 (90677)

b

Selected biosynthetic operons

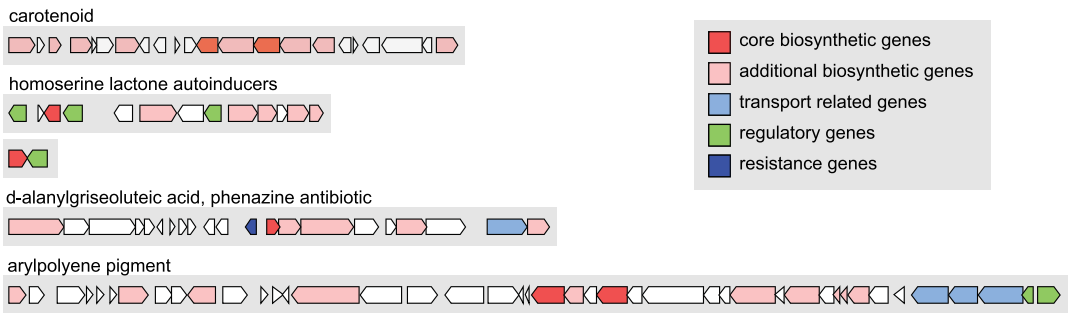

Extended Data Fig. 7 | Complete genome of *Pantoea agglomerans* ELM1. (**a**) The complete and closed genome of *P. agglomerans* ELM1 as well as two native plasmids. (**b**) Notable biosynthetic gene clusters present in the *P. agglomerans* ELM1 genome, including two pigment-producing biosynthetic clusters, which may be the source of the yellow tint of *P. agglomerans* ELM1 colonies, as well as an antibiotic-producing cluster and two quorum-sensing clusters that may contribute to *P. agglomerans* ELM1 capacity to dominate the hemp biomaterial during the growth phase.

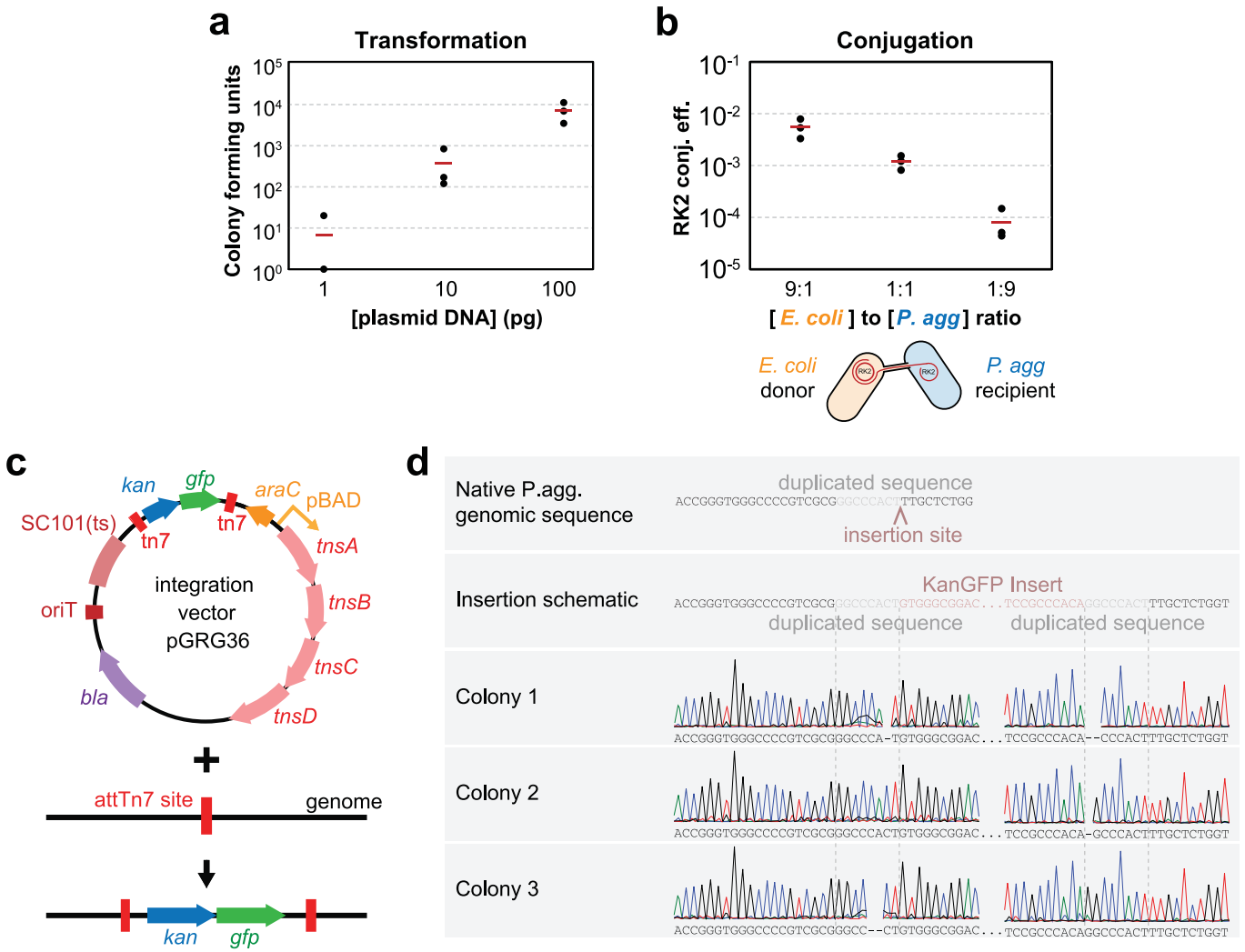

Extended Data Fig. 8 | Introduction of plasmids and genomic integration in *P. agglomerans ELM1*. (**a**) Plasmids can be readily transformed by electroporation into *P. agglomerans* ELM1 with standard protocols used in other Gram-negative Proteobacteria. (**b**) Plasmids can be efficiently transferred from donor *E. coli* bacteria into *P. agglomerans* ELM1 via bacterial conjugation using the RK2 system in a dosage dependent manner. The conjugation efficiency as measured by the number of transconjugants found compared to total recipients is shown. All data are triplicate biological samples (n = 3) with the mean shown as a red line. (**c**) Schematic of the pGRG vector, target genomic site at attTn7, and resulting integrant in the genome. (**d**) The Tn7 integration locus (attTn7), present in many *Enterobacteria*, is also found in *P. agglomerans* ELM1. Sequence verification of three colonies chosen from an integration experiment in *P. agglomerans* ELM1 using pGRG36, validating successful integration into the attTn7 site.

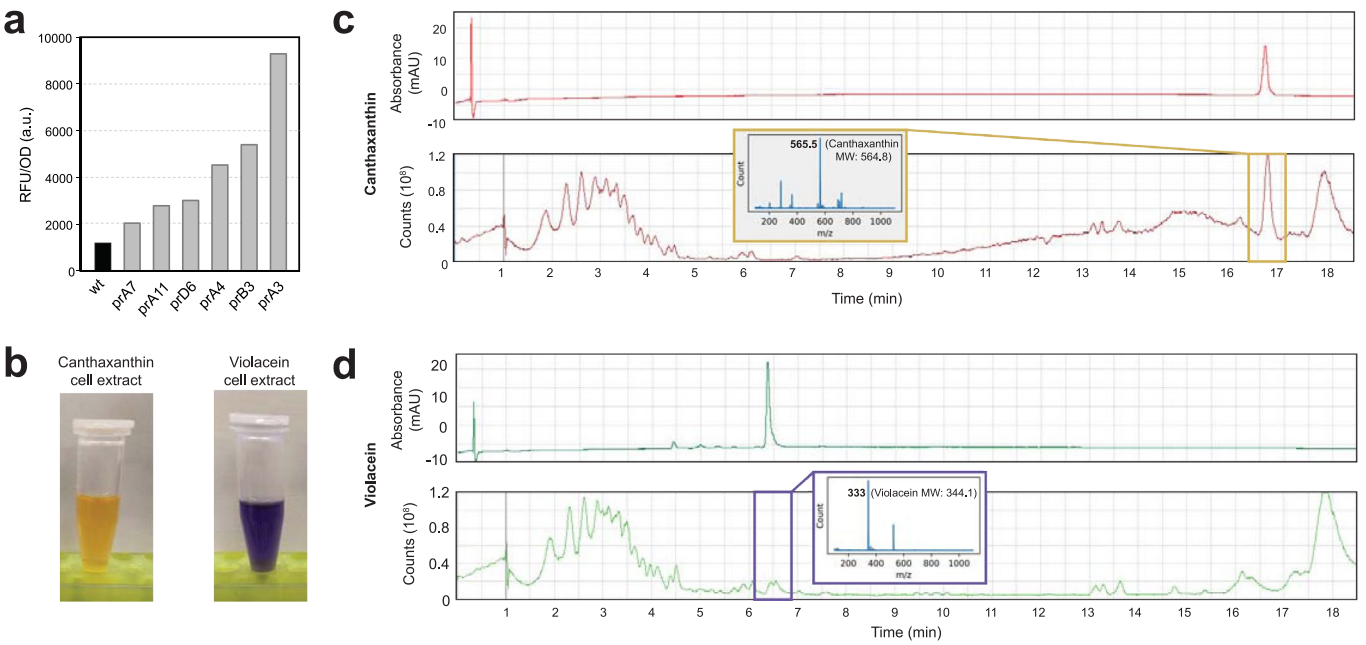

Extended Data Fig. 9 | Promoter characterization and canthaxanthin and violacein mass spectroscopy in *P. agglomerans* ELM1. (**a**) A set of constitutive promoters was cloned upstream of a GFP fluorescent reporter and transformed into *P. agglomerans* ELM1. Promoter activity as measured by Relative Fluorescence Units normalized to OD600 (RFU/OD) after 17 hours of growth in *P. agglomerans* ELM1 using a platereader. (**b**) Cell extracts of *P. agglomerans* ELM1 with colors characteristic of Canthaxanthin (left) and violacein (right) production. (**c**) Mass spectrometry of putatively canthaxanthin producing *P. agglomerans* ELM1 showing a single, clean absorbance spike at ~16.7 minute elution time and the corresponding mass spectra. (**d**) Violacein producer mass spec with a single, clean absorbance peak at 6.5 minute elution time and the corresponding mass spectra.

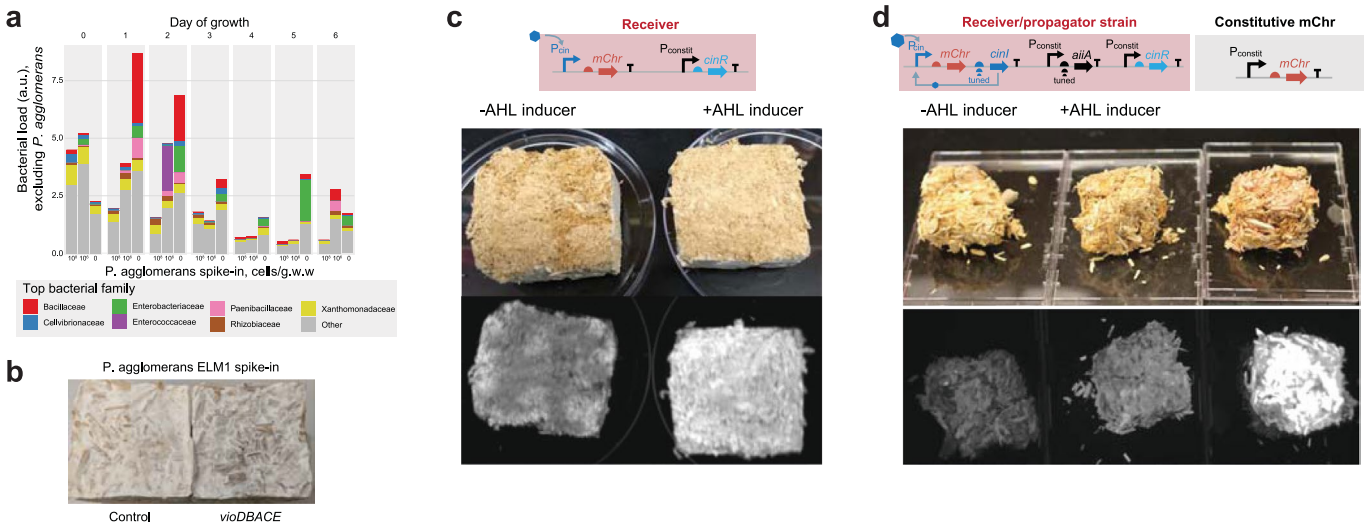

Extended Data Fig. 10 | Quorum sensing molecule-responsive living material blocks. (**a**) Absolute abundance sequencing of bacterial species in a growing living material block. Excluding *Pantoea* species from the analysis reveals that *P. agglomerans* ELM1 spike-in appears to outcompete other bacterial species and suppresses non-*Pantoea* bacterial density. (**b**) Spiking in an engineered *P. agglomerans* ELM1 strain carrying a violacein-producing plasmid pNM175 results in purple blocks with no noticeable decrease in *Ganoderma* growth. (**c**) When a *P. agglomerans* strain expressing mCherry in response to an AHL signal is spiked into the living material, blocks become responsive to AHL dosed into the material when blocks are generated. (**d**) Inclusion of the receiver/propagator strain into living material blocks renders the material sensitive to AHL added to the surface of the block at block generation time, but the output fluorescence is fainter compared to constitutive mCherry expression.

nature portfolio

Corresponding author(s): Harris Wang

Last updated by author(s): Aug 17, 2021

Reporting Summary

Nature Portfolio wishes to improve the reproducibility of the work that we publish. This form provides structure for consistency and transparency in reporting. For further information on Nature Portfolio policies, see our Editorial Policies and the Editorial Policy Checklist.

Statistics

For all statistical analyses, confirm that the following items are present in the figure legend, table legend, main text, or Methods section.

n/a	Confirmed	
☐	☒	The exact sample size (*n*) for each experimental group/condition, given as a discrete number and unit of measurement
☐	☒	A statement on whether measurements were taken from distinct samples or whether the same sample was measured repeatedly
☒	☐	The statistical test(s) used AND whether they are one- or two-sided *Only common tests should be described solely by name; describe more complex techniques in the Methods section.*
☒	☐	A description of all covariates tested
☒	☐	A description of any assumptions or corrections, such as tests of normality and adjustment for multiple comparisons
☐	☒	A full description of the statistical parameters including central tendency (e.g. means) or other basic estimates (e.g. regression coefficient) AND variation (e.g. standard deviation) or associated estimates of uncertainty (e.g. confidence intervals)
☒	☐	For null hypothesis testing, the test statistic (e.g. *F*, *t*, *r*) with confidence intervals, effect sizes, degrees of freedom and *P* value noted *Give P values as exact values whenever suitable.*
☒	☐	For Bayesian analysis, information on the choice of priors and Markov chain Monte Carlo settings
☒	☐	For hierarchical and complex designs, identification of the appropriate level for tests and full reporting of outcomes
☒	☐	Estimates of effect sizes (e.g. Cohen's *d*, Pearson's *r*), indicating how they were calculated

Our web collection on statistics for biologists contains articles on many of the points above.

Software and code

Policy information about availability of computer code

Data collection	A custom script was used in development of the signal propagation system design described in Figure 4, and is available is available at https://github.com/wanglabcumc/FungalBiocomposites.
Data analysis	Metagenomic sequences were processed using DADA2 vl.16, USEARCH 9.2.64, and Phyloseq 1.30.0. Isolates were identified using the SILVA and NCBI BLAST 16s webservers, accessed 04/2020. Pantoea agglomerans genome was assembled using Unicycler v0.4.9b and annotated using Prokka vl.12, antiSMASH web server vS.0.0, the dbcan2 webserver accessed 07/2019, CARD webserver accessed 04/2020, the EZbiocloud ANI webserver, accessed 06/2020 and NCBI BLAST, accessed 06/2020.

For manuscripts utilizing custom algorithms or software that are central to the research but not yet described in published literature, software must be made available to editors and reviewers. We strongly encourage code deposition in a community repository (e.g. GitHub). See the Nature Portfolio guidelines for submitting code & software for further information.

Data

Policy information about availability of data

All manuscripts must include a data availability statement. This statement should provide the following information, where applicable:

- Accession codes, unique identifiers, or web links for publicly available datasets
- A description of any restrictions on data availability
- For clinical datasets or third party data, please ensure that the statement adheres to our policy

Sequencing data generated for this study is deposited in the NCBI SRA at accession number PRJNA673748. Sequencing data associated with this study are deposited at NCBI SRA accession PRJNA673748. Metagenomic samples were classified against the SILVA database v132 and RDP Classifier training set 17 (16s) and UNITE database vl.12.17 (ITS). Raw data for F1b, c; F2f; F3b-d (and FED9a); FED1; FED3c; FED6a-c; FED8a, b; are included as Source Data files.

Field-specific reporting

Please select the one below that is the best fit for your research. If you are not sure, read the appropriate sections before making your selection.

☒ Life sciences ☐ Behavioural & social sciences ☐ Ecological, evolutionary & environmental sciences

For a reference copy of the document with all sections, see nature.com/documents/nr-reporting-summary-flat.pdf

Life sciences study design

All studies must disclose on these points even when the disclosure is negative.

Sample size	No sample size calculations were performed. Sequencing and material characterization experiments were derived from at minimum triplicate data to allow for generation of error bars.
Data exclusions	No data were exluded from this study.
Replication	Measurements of biomaterial mechanical performance were performed using three biological replicates. Sequencing samples were derived from at lease three biological replicates, excepting the absolute abundance spike-in experiment where each timepoint represents a single, independent batch. Pantoea agglomerans antibiotic sensitivity, plasmid copy number, carbon source utilization, transformation efficiency and conjugation experiments were performed with three biological replicates. Promoter strength data represents a single picked colony per promoter, evaluated using flow cytometry to visualize individual cell expression-level heterogeneity. Violacein and canthaxanthin expression mass spec experiments were performed with a single replicate, as they were qualitative descriptive experiments. In-block moisture, pH and ergosterol measurements were measured destructively using a block for each data point. All biomaterial block functionalization experiments were successfully replicated at least twice.
Randomization	No randomization was performed, as no experiments involved experimental groups.
Blinding	No blinding was performed, as no experiments involved group allocation.

Reporting for specific materials, systems and methods

We require information from authors about some types of materials, experimental systems and methods used in many studies. Here, indicate whether each material, system or method listed is relevant to your study. If you are not sure if a list item applies to your research, read the appropriate section before selecting a response.

Materials & experimental systems

n/a	Involved in the study
☒	☐ Antibodies
☒	☐ Eukaryotic cell lines
☒	☐ Palaeontology and archaeology
☒	☐ Animals and other organisms
☒	☐ Human research participants
☒	☐ Clinical data
☒	☐ Dual use research of concern

Methods

n/a	Involved in the study
☒	☐ ChIP-seq
☒	☐ Flow cytometry
☒	☐ MRI-based neuroimaging